Bioorganic & Medicinal Chemistry 28 (2020) 115544

Contents lists available at ScienceDirect

Bioorganic & Medicinal Chemistry

journal homepage: www.elsevier.com/locate/bmc

Design, synthesis and biological evaluation of novel pyrrolo[2,3-*d*] pyrimidine as tumor-targeting agents with selectivity for tumor uptake by high affinity folate receptors over the reduced folate carrier

Lalit K. Golani[a], Farhana Islam[a], Carrie O'Connor[b], Aamod S. Dekhne[b], Zhanjun Hou[b,d], Larry H. Matherly[b,c,d,1,*], Aleem Gangjee[a,1,*]

[a] Division of Medicinal Chemistry, Graduate School of Pharmaceutical Sciences, Duquesne University, 600 Forbes Avenue, Pittsburgh, PA 15282, United States
[b] Department of Oncology, Wayne State University School of Medicine, Detroit, MI 48201, United States
[c] Department of Pharmacology, Wayne State University School of Medicine, Detroit, MI 48201, United States
[d] Molecular Therapeutics Program, Barbara Ann Karmanos Cancer Institute, 421 East Canfield, Detroit, MI 48201, United States

ARTICLE INFO

Keywords:
Pyrrolo[2,3-*d*]pyrimidine
Heteroatom bridge
Folate receptor
Selective uptake
Reduced folate carrier

ABSTRACT

Tumor-targeted 6-substituted pyrrolo[2,3-*d*]pyrimidine benzoyl compounds based on **2** were isosterically modified at the 4-carbon bridge by replacing the vicinal (C11) carbon by heteroatoms N (**4**), O (**5**) or S (**6**), or with an *N*-substituted formyl (**7**), trifluoroacetyl (**8**) or acetyl (**9**). Replacement with sulfur (**6**) afforded the most potent KB tumor cell inhibitor, ~6-fold better than the parent **2**. In addition, **6** retained tumor transport selectivity via folate receptor (FR) α and -β over the ubiquitous reduced folate carrier (RFC). FRα-mediated cell inhibition for **6** was generally equivalent to **2,** while the FRβ-mediated activity was improved by 16-fold over **2**. N (**4**) and O (**5**) substitutions afforded similar tumor cell inhibitions as **2**, with selectivity for FRα and -β over RFC. The *N*-substituted analogs **7**–**9** also preserved transport selectivity for FRα and -β over RFC. For FRα-expressing CHO cells, potencies were in the order of **8** > **7** > **9**. Whereas **8** and **9** showed similar results with FRβ-expressing CHO cells, **7** was ~16-fold more active than **2**. By nucleoside rescue experiments, all the compounds inhibited *de novo* purine biosynthesis, likely at the step catalyzed by glycinamide ribonucleotide formyltransferase. Thus, heteroatom replacements of the CH_2 in the bridge of **2** afford analogs with increased tumor cell inhibition that could provide advantages over **2**, as well as tumor transport selectivity over clinically used antifolates including methotrexate and pemetrexed.

1. Introduction

Reduced folates (e.g. 5-methyltetrahydrofolate) play critical roles as cofactors in the biosynthesis of purines and pyrimidines.[1,2] Mammalian cells lack the enzymatic machinery to synthesize folates *de novo*. As a result, it is necessary to obtain folates from dietary sources. Folate cofactors are bivalent anions and hydrophilic compounds that diffuse poorly across cell membranes. Reflecting this, specific transport systems are needed to achieve sufficient intracellular concentrations of folates to support cellular anabolism.[3]

Three specialized folate transport systems exist in mammalian cells that include the reduced folate carrier (RFC),[4] folate receptors (FRs) α and β,[5] and the proton-coupled folate transporter (PCFT).[6–8] RFC and PCFT are facilitative folate transporters,[4,7] whereas FRs are glycosyl

Abbreviations: (AICA), 5-Aminoimidazole-4-carboxamide; (AICARFTase), 5-aminoimidazole-4-carboxamide ribonucleotide formyltransferase; (CHO), Chinese hamster ovary; (FBS), fetal bovine serum; (FDA), Food and Drug Administration; (FF), folate free; (FR), folate receptor; (10-CHOTHF), N10-formyl tetrahydrofolate; (GAR), glycinamide ribonucleotide; (GARFTase), glycinamide ribonucleotide formyltransferase; (GPI), glycosyl-phosphatidylinositol; (IC_{50}), 50 percent inhibitory concentration; (IUPAC), Chemical names follow International Union of Pure and Applied Chemistry; (LCV), leucovorin; (MHz), megahertz; (MTX), methotrexate; (MEM), minimal essential media; (NMR), nuclear magnetic resonance spectra; (NSCLC), non-small cell lung cancer; (*N*-CHO), N- formyl; (N-$COCF_3$), *N*-trifluoroacetyl; (N-$COCH_3$), *N*-acetyl; (ppm), parts per million; (PMX), pemetrexed; (PCFT), proton-coupled folate transporter; (RTX), Raltitrexed; (RFC), reduced folate carrier; (RMSD), root-mean-square deviation; (RPMI), Roswell Park Memorial Institute; (TLC), thin layer chromatography; (UV), ultraviolet

* Corresponding authors at: Division of Medicinal Chemistry, Graduate School of Pharmaceutical Sciences, Duquesne University, 600 Forbes Avenue, Pittsburgh, PA 15282, United States (A.Gangjee); Barbara Ann Karmanos Cancer Institute, 421 East Canfield, Detroit, MI 48201, United States (L.H. Matherly).
E-mail addresses: lalit2510@gmail.com (L.K. Golani), matherly@karmanos.org (L.H. Matherly), gangjee@duq.edu (A. Gangjee).
[1] To whom correspondence should be addressed.

https://doi.org/10.1016/j.bmc.2020.115544
Received 16 December 2019; Received in revised form 29 April 2020; Accepted 30 April 2020
Available online 06 May 2020
0968-0896/

phosphatidylinositol-linked proteins that mediate uptake of folates into cells by receptor-mediated endocytosis.[5] RFC is the major route for membrane transport of circulating folates into mammalian tissues. RFC is expressed in both normal and cancer cells, whereas FRα, FRβ, and PCFT exhibit narrower patterns of tissue expression and serve more specialized physiological roles.[4,5,7,8] RFC functions optimally at neutral pH (~7.4) associated with most normal tissues.[4]

PCFT is expressed at apical brush border membranes of the duodenum and proximal jejunum where it functions at low pH and is the major intestinal transporter for the absorption of dietary folates.[9,10] Although PCFT can be detected in other tissues (e.g., liver, kidney),[8] the requirement for an acidic pH (pH < 7, optimum at pH 5–5.5) for optimal activity[7,10] precludes significant levels of PCFT transport in most normal tissues.[6]

For over 60 years, antifolates have served important therapeutic roles as anticancer, antimicrobial and immunomodulatory agents.[11–13] Methotrexate (MTX), a dihydrofolate reductase inhibitor, is a well-known classical antifolate and continues to be used to treat acute lymphoblastic leukemia and rheumatoid arthritis.[13] Other clinically used antifolates include pralatrexate, a DHFR inhibitor used for peripheral *T*-cell lymphoma,[12] and the thymidylate synthase inhibitors raltitrexed (for colorectal cancer) and pemetrexed (PMX) (for non-small cell lung cancer (NSCLC) and malignant pleural mesothelioma) (Fig. 1).[14] PMX also inhibits secondary targets in one-carbon metabolism, including glycinamide ribonucleotide (GAR) and 5-aminoimidazole-4-carboxamide (AICA) formyltransferases (GARFTase and AICARFTase, respectively) in *de novo* purine biosynthesis, and DHFR.[14] As all of these antifolates are excellent substrates for cellular uptake by the ubiquitously expressed RFC, they are comparatively nonselective for tumors versus normal tissues and show dose-limiting toxicities when used as cancer chemotherapeutic agents, resulting in tumor resistance and in some cases treatment failures.[4,8,15]

There has been an increased recognition of human FRs as targets for the specific delivery of new classes of antifolates or folate conjugates to tumors or sites of inflammation.[16–18] In humans, three genes encoding functional FRs termed FRα, FRβ, and FRγ have been recognized.[5,19,20] FRα and FRβ are anchored at the plasma membrane via a glycosylphosphatidylinositol (GPI)- anchor, whereas FRγ is secreted due to the lack of a signal sequence for GPI anchor attachment.[5] FRα is detected on apical surfaces of several epithelial cells (e.g., kidney) where it is inaccessible to parenterally administered folates and related compounds.[5] FRβ is detected in spleen, bone marrow, and thymus[5].

Moreover, in many types of cancer and inflammatory diseases, reflecting high expression levels of FRα or FRβ, FR-targeted therapies are expected to be effective.[5,17,18,21,22] FR-targeted therapeutics are predicted to show modest toxicity in normal tissues because of the restricted expression of both FRα and FRβ, and for FRα, limited access to the circulation.[5,17–19,23] FRα has been reported to be highly expressed in adenocarcinomas of the ovary, lung, uterus, breast, cervix, kidney, and colon, as well as testicular choriocarcinoma, ependymal brain tumors, and nonfunctioning pituitary adenocarcinoma.[5,17–19,21,24] For certain leukemias, such as chronic myelogenous leukemia and acute myelogenous leukemia, FRβ expression is elevated.[25] FRβ is also expressed in tumor-associated macrophages[20], and activated synovial macrophages involved in the pathogenesis of rheumatoid arthritis[26] and other inflammatory conditions including psoriasis and Crohn's disease.[20,27] Finally, FRβ has been reported in gastric acid cancer and multiple myeloma, along with other human neoplastic tissues.[24,28,29]

FR-targeted therapeutics based on FR-targeted antibodies, folate-conjugates, and antifolates are being pursued.[18] A FRα-targeting antibody-drug conjugate mirvetuximab soravtansine (IMGN853; ImmunoGen)[30] received "Fast Track" designation by the US Food and Drug Administration (FDA) and entered Phase III clinical trials. FRα-targeted strategies have used folate conjugates to deliver toxins, liposomes, and cytotoxic agents to FRα-expressing tumors.[15] Clinically tested therapies include EC1456, a folic acid-tubulysin conjugate.[17,31] ONX-0801 (BGC 945), a thymidylate synthase (TS) inhibitor,[16] completed a Phase I clinical trial with plans for a randomized biomarker pre-specified Phase II clinical trial.[32]

We discovered 6-substituted 2-amino-4-oxo pyrrolo[2,3-*d*]pyrimidines as inhibitors of tumor cell proliferation with cellular uptake by FRs and PCFT and inhibition of *de novo* purine biosynthesis at the first folate-dependent step catalyzed by GARFTase.[33–41] Among the most active analogs of the previously published series were compounds **1** and **3** (Fig. 2), both three atom bridged compounds, with selective transport into certain tumor cells by FRs and PCFT (Table 1). Upon internalization, compounds **1** and **3** inhibited GARFTase in *de novo* purine nucleotide biosynthesis, resulting in depletion of purine nucleotides.[33,42] However, for compounds **1** and **3**, selectivity over RFC was less than absolute.[35,42] The non-selective activity of these 3-atom bridged analogs may reflect their shorter bridge lengths, which are similar to those for 2-atom bridged classic antifolate drugs such as MTX and PMX which are good RFC substrates and are poor (and non-selective) substrates for FRs.[35,42]

Compound **2** is an analog of **1** but it has a 4-carbon bridge and showed better selectivity for FRs and PCFT than **1** or **3**.[35,42] The length of the side chains in the carbon-bridged analogs was previously identified as an important structural determinant of potency and transport selectivity.[35,40,42] For analogs with bridge lengths from 2 to 8 carbons, the most potent tumor inhibitors had 3 carbons (e.g., compound **1**) (Fig. 2). However, this was at the expense of transport selectivity.[33,42] For the 4-carbon bridge analogs like **2**, there was an improvement in FR selectivity over RFC compared to **1** without loss of anti-tumor activity; however, this was accompanied by decreased PCFT activity.[33,42]

We reported[35] that the replacement of the benzylic carbon in **1** (3-carbon bridge) (Fig. 2) with a heteroatom (N, O or S) provides a series

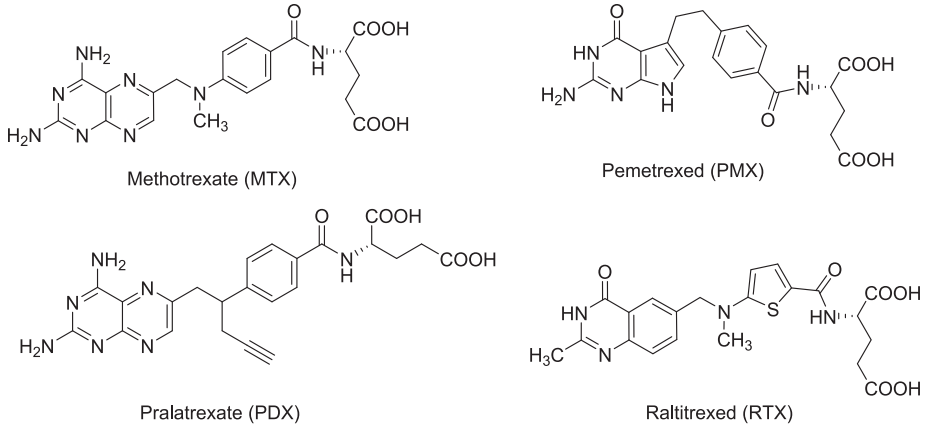

Fig. 1. Structures of classical antifolate drugs, including methotrexate (MTX), pemetrexed (PMX), pralatrexate (PDX), and raltitrexed (RTX).

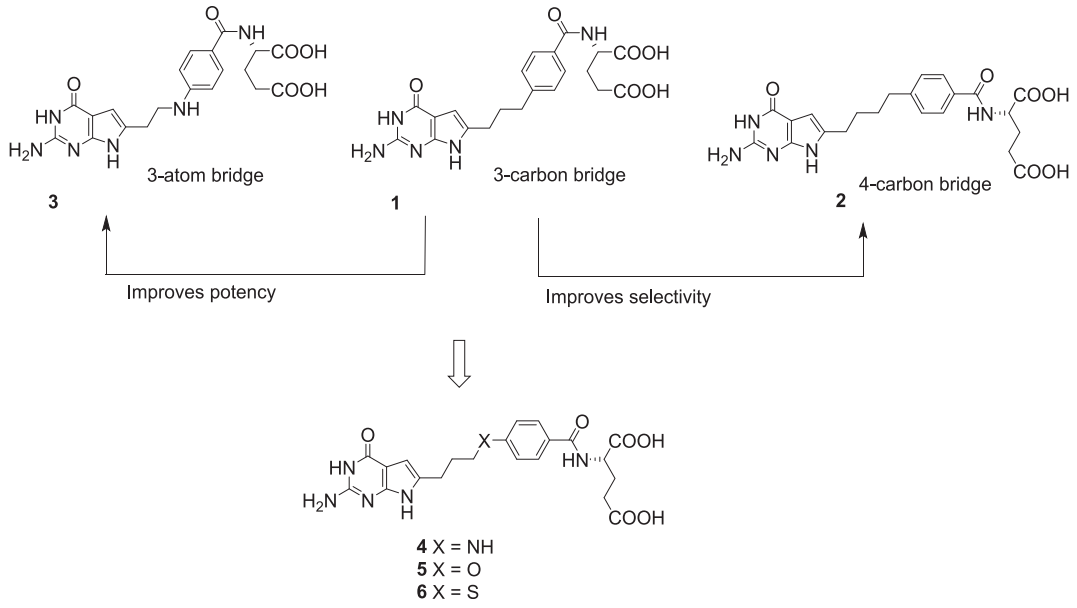

Fig. 2. Design of compounds with optimized chain lengths.

of compounds that were more potent toward FRα-expressing KB human tumor cells, with substantial selectivity for FRs and PCFT over RFC.[35] Analysis of the X-ray crystal structures of the bridge with a *N*-atom analog **3** (Fig. 2) with human FRα and GARFTase showed that the bound conformations required flexibility to attach to both FRα (PDB 5IZQ) and GARFTase (PDB 5J9F).[35] The X-ray crystal structure of **3** with GARFTase showed that the bridge heteroatoms of the bound inhibitor formed intermolecular interactions with GARFTase, mediated by an ordered water molecule (PDB 5J9F).[35] Analogs of **3** with *N*-formyl (*N*-CHO), *N*-trifluoroacetyl (N-$COCF_3$), or *N*-acetyl (N-$COCH_3$) substitutions were designed to mimic the GARFTase substrate (*N*10-formyl tetrahydrofolate; 10-CHO-THF) (Fig. 3) and to afford additional hydrogen bonding within the GARFTase active site.[35] Compound **3,** in addition to tumor cell inhibition, was also efficacious *in vivo* in mice bearing IGROV1 ovarian tumor xenografts.[35]

Thus, it was of interest to synthesize 4-atom bridged compounds with heteroatoms (N, O, S, and N-CHO, N-$COCF_3$, N-$COCH_3$) (Figs. 2 and 3) as hybrids of the 4-carbon bridged analog **2** that improves transport selectivity, and the heteroatom bridged analog **3** that increases potency towards tumor cells. These hybrid analogs were expected to afford improved antitumor potencies and transporter selectivities, compared to PMX. This is anticipated to overcome toxicity and potential resistance to PMX. The current work involves the synthesis of pyrrolo[2,3–*d*]pyrimidine analogs with the benzylic CH_2 of the 4-carbon bridge of **2** replaced with NH (**4**), O (**5**), or S (**6**) (Fig. 2). We measured the bond lengths and bond angles in compounds **4–6** and compared them with literature values.[43] As flexibility is crucial for the binding to both FRα (PDB 5IZQ) and GARFTase (PDB 5J9F),[35] it is notable that the increased bond length of **6** (2.93 Å) compared to **2** (2.55 Å) (Fig. 4) provides additional flexibility in the chain region to afford both FRα (PDB 5IZQ) selectivity over RFC and GARFTase potency. The bond angle of C—S—C in **6** (109.1°) is decreased compared to C—C—C (112.8°)[44] in **2** (Fig. 4), which is responsible for a different conformation and orientation of the α and γ-carboxylates of the L-glutamate of **6** compared to **2**. Compounds **4** and **5** have comparable bond lengths and bond angles to **2** and are predicted to mimic compound **2**

Table 1
IC_{50}s (in nM) for 6-substituted pyrrrolo[2,3–*d*]pyrimidine benzoyl antifolates with heteroatom replacements, and classical antifolates in RFC-, PCFT- and FR-expressing cell lines. Proliferation assays were performed for CHO sublines engineered to express human RFC (PC43-10), FRα (RT16), FRβ (D4) or PCFT (R2/PCFT4), and transporter-null (R2) CHO cells, and KB human tumor cells (express RFC, FRα, and PCFT). For the experiments measuring FR-mediated effects, assays were performed in the presence or absence of 200 nM folic acid (results are shown only for KB cells). Results are presented as IC_{50} values, corresponding to the concentrations that inhibit growth by 50% relative to cells incubated without the drug. The data are mean values from 5 to 16 experiments (± standard errors in parentheses). Some of the data for **3**, MTX, and PMX have been previously published.[35,51] Results are also summarized for KB cells for the protective effects of adenosine (60 μM), thymidine (10 μM), glycine (130 μM) or 5-aminoimidazole-4-carboxamide (320 μM). For compounds **2**, **4**, **5**, **6**, **7**, **8**, and **9**, folic acid and nucleoside/AICA protection results are shown in Fig. 7. Methods are summarized in the Experimental Section. Undefined abbreviations: Ade, adenosine; AICA, 5-aminoimidazole-4-carboxamide; FA, folic acid; gly, glycine; ND, not determined; and Thd, thymidine.

Compounds	R2	RFC	FRα	FRβ	PCFT	RFC/FRα/PCFT		
		PC43-10	RT16	D4	R2/PCFT4	KB	KB (+FA)	KB + Ade/Thd/AICA/gly
1	> 1000	649(38)	4.1(1.6)	5.6(1.2)	23.0(3.3)	1.7(0.4)	> 1000	Ade/AICA
2	> 1000	> 1000	6.3(1.6)	10(2)	213(28)	1.9(0.7)	> 1000	Ade/AICA
3	> 1000	510(90)	3.04 (0.71)	0.62(0.20)	87.4(9.9)	0.32(0.05)	666(46)	Ade/AICA
4	697(1 5 8)	670(1 5 0)	1.76(0.43)	1.51(0.43)	235(96)	0.95(0.35)	> 1000	Ade/AICA
5	> 1000	> 1000	4.6(1.3)	5.6(1.4)	> 1000	2.50(0.64)	> 1000	Ade/AICA
6	> 1000	> 1000	2.56(0.73)	0.60(0.12)	593(2 0 4)	0.30(0.04)	757(41)	Ade/AICA
7	> 1000	> 1000	35.63 (4.78)	0.61 (0.11)	893(1 6 1)	13.20 (3.32)	> 1000	Ade/AICA
8	> 1000	> 1000	5.78(1.45)	3.87(0.54)	487(1 7 1)	5.35 (0.49)	> 1000	Ade/AICA
9	> 1000	> 1000	57.24 (6.9)	12.79 (1.90)	> 1000	40.11 (9.34)	> 1000	Ade/AICA
MTX	216(8.7)	12(1.1)	114(31)	106(11)	121(17)	6.00(0.60)	20(2.4)	Thd/Ade
PMX	894(93)	138(13)	42(9)	60 (8)	13.2(2.4)	68(12)	327(1 0 3)	Thd/Ade

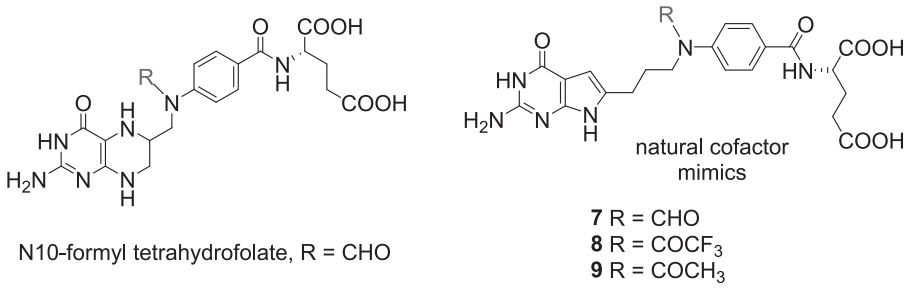

Fig. 3. Structure of *N10*-formyl tetrahydrofolate and proposed mimics.

(Fig. 4). The purpose of this study is to determine the effects of heteroatom replacements of the vicinal (C11) carbon to the side chain phenyl ring in compound **2** by N, O, or S, and N-CHO, N-$COCF_3$, or N-$COCH_3$ moieties (7–9) on transport specificities by FRα, FRβ, and PCFT, over RFC, and on the inhibition of *de novo* purine nucleotide biosynthesis on cell proliferation and antitumor activity.

2. Molecular modeling

To determine the ligand-protein interactions, docking studies were carried out with compounds **4–9** using X-ray crystal structures of human GARFTase (PDB 5J9F), FRα (PDB 5IZQ) and FRβ (PDB 4KN2).[23,35,37,45] Docking scores are provided in supporting information (Table 2S).

2.1. Docking studies of compounds 4–9 with human GARFTase (PDB: 5J9F) (Figs. 5A and 5B):

Docking results of compounds **2**, **4**, and **6** with human GARFTase (PDB 5J9F) are displayed in Figs. 5A and 5B. The docked poses of **2**, **4** and **6** indicate that the pyrrolo[2,3–*d*]pyrimidine scaffold is buried in the active site and occupies the same location as the bound ligand **3**[35] (Figs. 5A and 5B; bound ligand **3** not shown for clarity). The bicyclic pyrrolo[2,3–*d*]pyrimidine scaffold of **4** and **6** is stabilized by the hydrogen bonding interactions, including hydrogen bonds between the N1 nitrogen and the backbone amide −NH− of Leu899 and the 2-NH_2 and the backbone carbonyls of Glu948 and Leu899. Other interactions include N3 and the backbone carbonyl of Ala947, and the 4-oxo and the backbone −NH- of Ala947 and Val950. The N11-H of compound **4** is hydrogen-bonded via a water-mediated hydrogen-bond with the substrate GAR (Fig. 5A). Similar interactions are predicted to occur involving the heteroatom bridge of **5** (oxygen) (figure not shown). The flexible four-atom bridges of **4** and **6** orient the side chain phenyl ring into a hydrophobic cleft comprised of Phe895 (not labeled), Met896, Leu899, and Ile898. The interactions involving the flexible glutamate side chains are similar to those reported for the glutamate side chain of **3**.[35] The α-carboxylic acid of **4** forms salt bridges with Arg871 and Arg897, and hydrogen bonds with the backbone of Ile898. The γ-carboxylic acid forms a salt bridge with Lys844 and Arg897 (Fig. 5A). Compounds **2** and **4** had docked scores of −14.02 and −14.29 kcal/mol, respectively, in GARFTase, similar to that for **3** (-14.36 kcal/mol). Docking studies of **6** suggested an altered orientation of the phenyl ring and side-chain L-glutamate compared to **4**. This is attributed to the larger size of the sulfur atom, resulting in a different set of interactions between the active site with the L-glutamate side chain of **6**. The α-carboxylic acid forms a salt bridge with Arg897, while the γ-carboxylic acid of **6** forms a salt bridge with Arg871 (Fig. 5B). The resulting docking score of **6** is −14.53 kcal/mol, somewhat better than **2–4**, indicating an increased inhibition of GARFTase. The N11-CHO, $COCF_3$, and $COCH_3$ moieties in **7**, **8**, and **9**, respectively, are oriented similarly

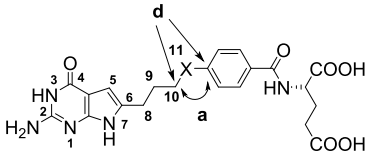

Comp.	X	Distance (d)[44]	Angle (a)[44]
2	CH_2	2.55 Å	112.8°
4	NH	2.50 Å	121.9°
5	O	2.42 Å	119.4°
6	S	2.93 Å	109.1°

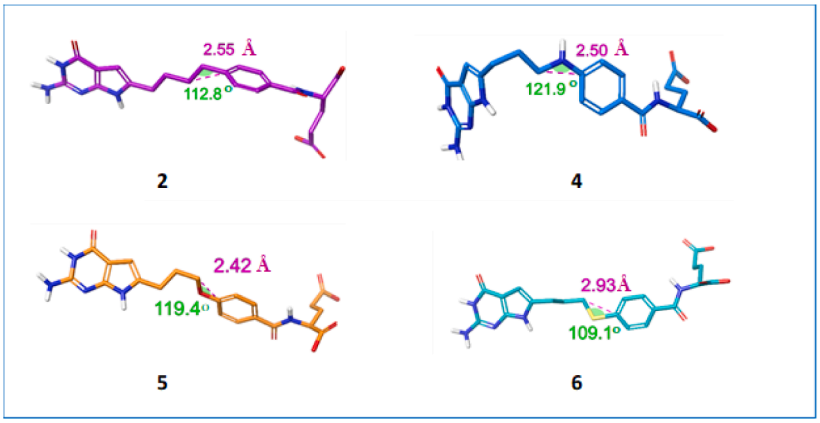

Fig. 4. Distance and bond angle variations predicted by the nature of the bridge at the benzylic position (X). Distances and angles for X = NH, O, and S were measured using energy-minimized conformations of compounds with Maestro Schrödinger 2019-1.[44]

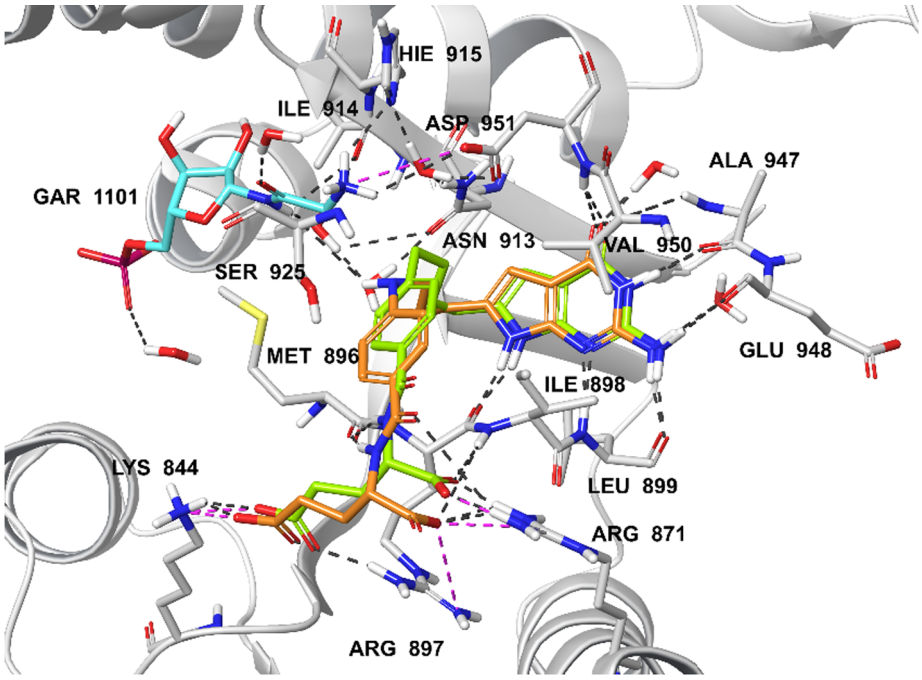

Fig. 5A. Molecular modeling studies with human GARFTase (PDB 5J9F).[33] Superimposition of the docked pose of **2** (green), **4** (tan) and GAR (cyan). Docking scores of **2** and **4** are −14.02 and −14.29 kcal/mol, respectively. Hydrogen bond interactions, pi-pi interactions, and salt bridges are depicted as black, cyan and magenta dashed lines, respectively.

to the N11-H of **4**. Compounds **7–9** bind deeper into the formyl transfer region that is occupied by the formyl group of the natural GARFTase substrate, N10-formyl tetrahydrofolate (10-CHOTHF) (figure not shown). The docked scores of **5** and **7–9** (-14.38, −14.79, −14.87, and −14.12 kcal/mol, respectively), are equivalent to that for **4** (-14.29 cal/mol), which suggest that these compounds should be potent GARFTase inhibitors.

2.2. Docking studies of compound 4–9 with FRα (PDB 5IZQ) and FRβ (PDB 4KN2) (Figs. 6A-6C):

The docked poses of **2, 4** and **6** with the crystal structures of **3** in FRα (PDB 5IZQ)[35,45] and PMX in FRβ (PDB 4KN2)[23] indicated that all three compounds are accommodated within a similar space as **3** and PMX, respectively (Figs. 6A, 6B, 6C; **3** and PMX are not shown for clarity). Figs. 6A and 6B display the docked poses of compounds **2**, **4** and **6** in the X-ray crystal structures of human FRα. Molecular modeling revealed that the pyrrolo[2,3–*d*]pyrimidine scaffold of compounds **4** and **6** are stacked between the side chains of Tyr85 and Trp171, similar to the bicyclic scaffold of bound ligand **3** (Figs. 6A and 6B; **3** not shown for clarity).[35] The 2-NH_2 and 7-NH of compounds **4** and **6** form hydrogen bonds with Asp81. Additional hydrogen bonds are formed between N3 and Ser174, and between the 4-oxo group and side chains of Arg103 and Arg106. The α-carboxylic acids of **4** and **6** form hydrogen bonds with the backbone NH of Gly137 and the pyrrole NH of Trp140, while the γ-carboxylic acid forms a salt bridge with Lys136. In comparison, with the 3-atom linker of **3** (not shown for clarity), the four atom linkers of **4** and **6** position the phenyl ring in the hydrophobic

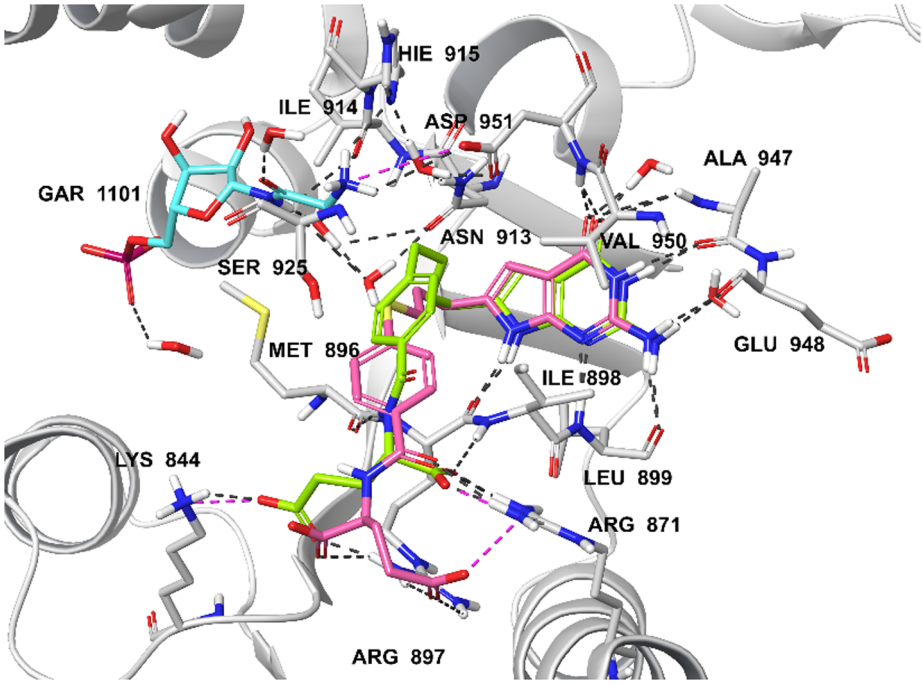

Fig. 5B. Molecular modeling studies with human GARFTase (PDB 5J9F).[33] Superimposition of the docked pose of **2** (green), **6** (pink) and GAR (cyan). Docking scores of **2** and **6** are −14.02 and −14.53 kcal/mol, respectively. Hydrogen bond interactions, pi-pi interactions, and salt bridges are depicted as black, cyan, and magenta dashed lines, respectively.

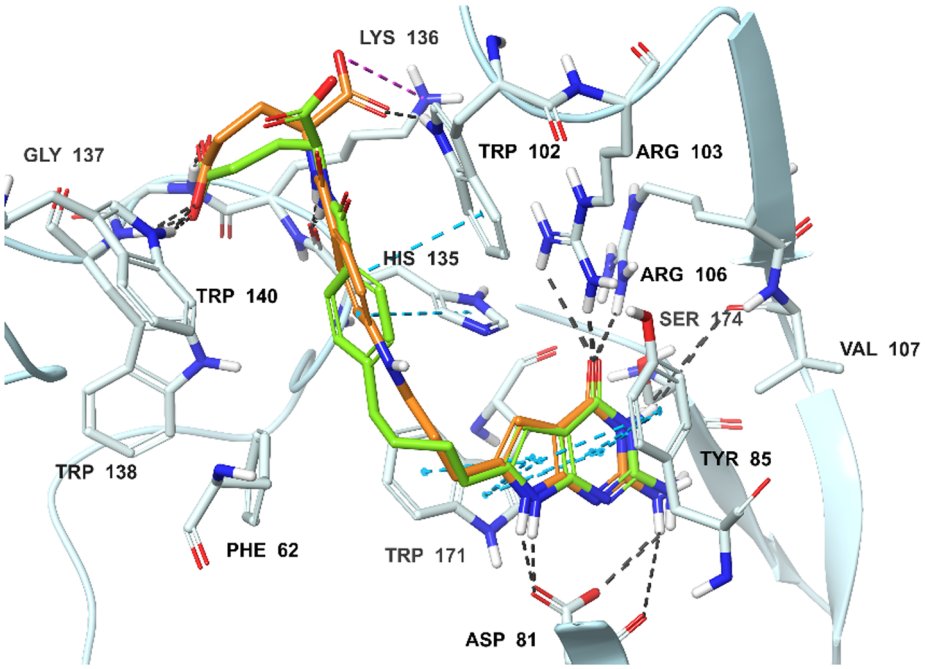

Fig. 6A. Molecular modeling studies using the human FRα (PDB 5IZQ)[35,46] crystal structures. Superimposition of the docked pose of **2** (green) with the docked pose of **4** (tan) in FRα. Docking scores of **2** and **4** are −11.72 and −12.02 kcal/mol, respectively. Hydrogen bonding interactions, pi-pi interactions, and salt bridges are depicted as black cyan and magenta dashed lines, respectively.

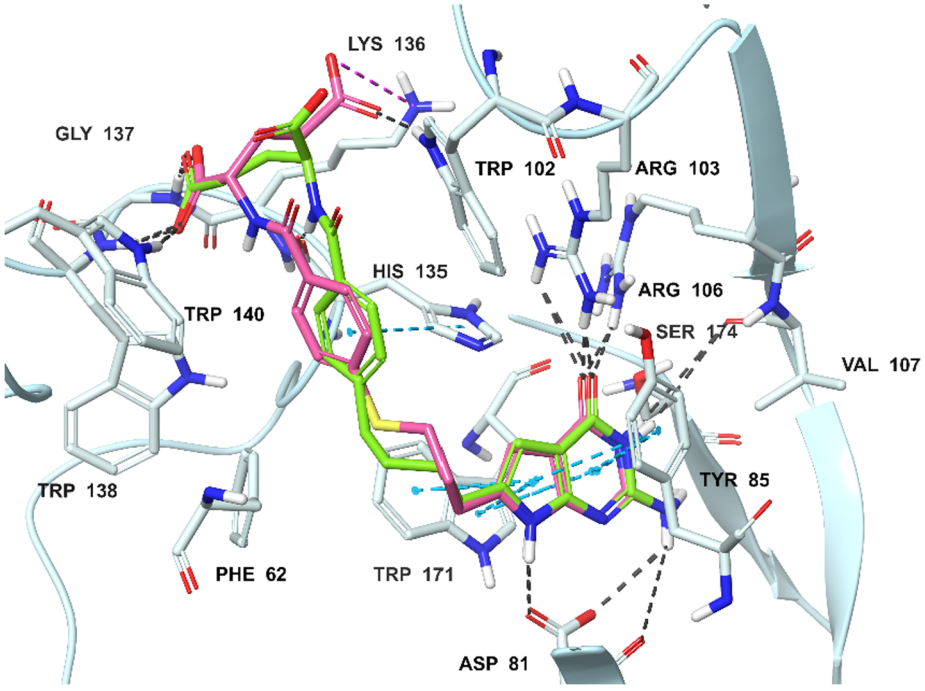

Fig. 6B. Molecular modeling studies using the human FRα (PDB 5IZQ)[35,46] crystal structures. Superimposition of the docked pose of **2** (green) with the docked pose of **6** (pink) in FRα. Docking scores of **2** and **6** are −11.72 and −12.07 kcal/mol, respectively. Hydrogen bondinteractions, pi-pi interactions, and salt bridges are depicted as black, cyan and magenta dashed lines, respectively.

pocket (Tyr60, Trp102, His135, and Trp138) to make hydrophobic interactions (Figs. 6A and 6B). The results revealed that the expanded chain length in the 4-atom chain compound (compared to **3**) is vital for positioning the phenyl ring to the hydrophobic pocket for increased FRα selectivity.

Figs. 6C shows the docked pose of compounds **2** and **6** in the X-ray crystal structure of human FRβ (PDB 4KN2).[23] In this pose, the orientation of the scaffold permits the 2-NH_2 and 7-NH moieties of both **2** and **6** to form hydrogen bonds with Asp97, and the 4-oxo moiety to form hydrogen bonds with the side-chain nitrogen hydrogens of Arg119, His151 and Tyr101. Hydrogen bonding interaction with Ser190 and N3 of **2** and **6** were also observed. The pyrrolo[2,3–*d*] pyrimidine scaffold is stacked amid the hydrophobic aromatic side chains of Tyr101 and Trp187. The L-glutamate moiety occupies a similar binding space as the corresponding L-glutamate of the native ligand.[35] The α-carboxylate forms a salt bridge with Arg152 and hydrogen bonds with the pyrrole NH of Trp118, while the γ-carboxylic acid of **2** and **6** forms hydrogen bonds with the pyrrole NH of Trp156 and a water-mediated hydrogen bond with the backbone of Trp154. The flexible four atom bridge with the sulfur atom of **2** and **6** helps to orient the side chain phenyl ring into a hydrophobic cleft of amino acids Phe78, Trp118, and Trp154. The extended chain length (4-atom chain) provides FRβ selectivity, mediated by these hydrophobic interactions. These interactions are less apparent in the 3-atom chain compound **3** (not shown for clarity).

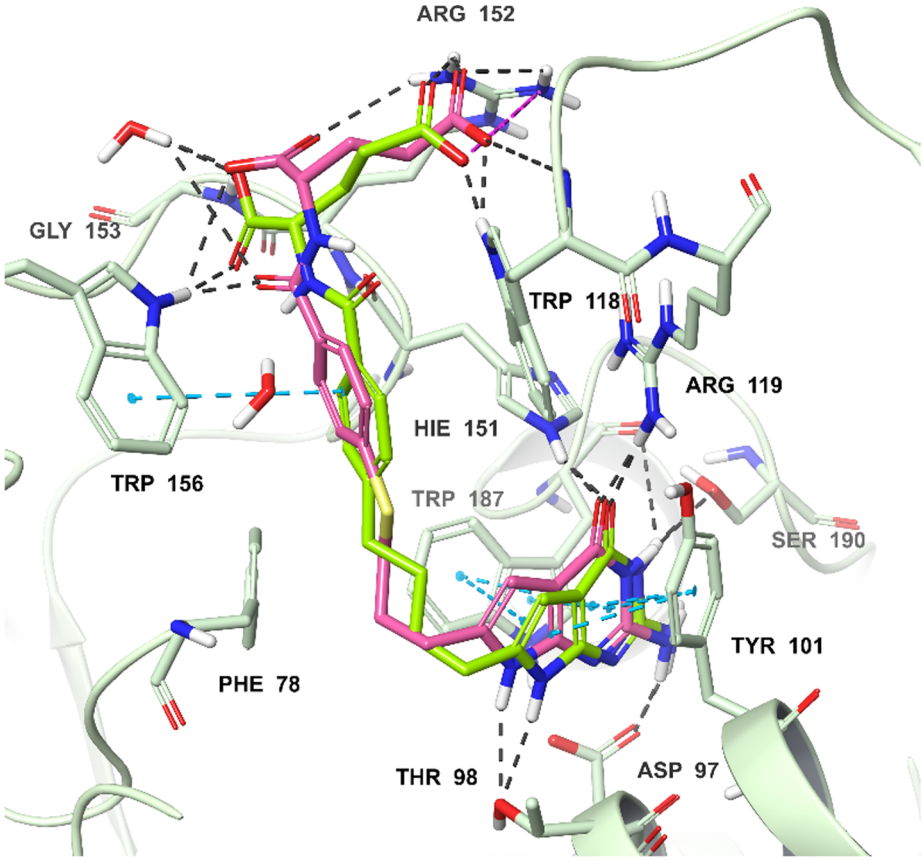

Fig. 6C. Molecular modeling studies using the human FRβ (PDB 4KN2)[23] crystal structures. Superimposition of the docked pose of **2** (green) with the docked pose of **6** (pink) in FRβ. Docking scores of **2** and **6** are −13.92 and −14.84 kcal/mol, respectively. Hydrogen bonding interactions, pi-pi interactions, and salt bridges are depicted as black, cyan and magenta dashed lines, respectively.

3. Chemistry

The reaction of *β*-propiolactone **10** (Scheme 1) and ethyl *p*-aminobenzoate **11** afforded **12**.[46] The carboxylic acid **12** was then treated with trifluoroacetic anhydride to give the protected amine **13**.[35] Compound **13** was converted to the acid chloride and immediately reacted with diazomethane, followed by treatment with silver acetate to provide the homologated carboxylic acid **14**. Carboxylic acid **14** was then converted to the acid chloride and immediately reacted with diazomethane, followed by 48% HBr in water to afford the α-bromoketone **15**. Condensation of 2,6-diamino-3*H*-pyrimidin-4-one with **15** in DMF at room temperature for 3 days provided the 6-substituted-2-amino-4-oxo-pyrrolo[2,3–*d*]pyrimidine **16**. Hydrolysis of **16** resulted in the corresponding free acid **17**. Subsequent coupling with L-glutamate dimethyl ester using 2-chloro-4,6-dimethoxy-1,3,5-triazine as the activating agent provided the diester **18**. Saponification of the diester yielded the target **4**. Compound **4** was then reacted with formic acid, trifluoroacetic anhydride or acetic anhydride to afford target compounds **7**, **8** and **9**, respectively.

The carboxylic acids **22** and **23** (Scheme 2) were obtained *via* nucleophilic substitution of the alkyl bromide **19** with **20** or **21**, respectively, followed by deprotection of the *tert*-butyl ester with trifluoroacetic acid.[47] Compounds **22** and **23** were then converted to the acid chloride and immediately reacted with diazomethane, followed by 48% HBr in water to provide the corresponding *α*-bromomethylketones **28** and **29**, respectively.[35] Condensation of 2,6-diamino-3*H*-pyrimidin-4-one with **28** and **29** in DMF at room temperature for 3 days afforded the 2-amino-4-oxo-6-substituted-pyrrolo[2,3–*d*]pyrimidines **30** and **31**, respectively. Hydrolysis of **30** and **31** afforded the corresponding free acids **32** and **33**, respectively. Subsequent coupling with L-glutamate ester using 2-chloro-4,6-dimethoxy-1,3,5-triazine as the activating agent provided the diesters **34** and **35**. Saponification of the diesters yielded the target compounds **5** and **6**.

4. Biological evaluation and discussion

As a part of the study of structure-activity relationships for tumor-targeted antitumor compounds with specificities for the individual transporters, we measured the impact of isosteric heteroatom replacements, including N, O, and S (compounds **4**, **5**, and **6**, respectively), of CH_2 at position-11 (compound **2**) (Fig. 2). Additional *N*-substituted analogs related to **4** with formyl (**7**), trifluoroacetyl (**8**), and acetyl (**9**) substitutions (Fig. 3), as a mimic of the natural substrate, 10-CHOTHF cofactor for GARFTase, were also tested.

To screen for antiproliferative activities, we used a panel of isogenic Chinese hamster ovary (CHO) sublines engineered from RFC-, FR- and PCFT-null MTXRIIOua^{R}2-4 CHO cells[48] (R2) cells to individually express FRα (RT16 cells), FRβ (D4), RFC (PC43-10), or PCFT (R2/PCFT4).[33,42,49,50] The CHO cells were cultured with a range of drug concentrations for up to 96 h and cell viabilities were measured to calculate IC_{50} values, corresponding to the concentrations that inhibit growth by 50%.[42] Results are summarized in Table 1 and are compared to the inhibition of FRα-expressing KB human tumor cells.

The 6-substituted pyrrolo[2,3–*d*]pyrimidine analogs with heteroatom bridge replacements, **4** (N), **5** (O), and **6** (S), all showed potent growth inhibition toward FRα-expressing RT16 cells and toward FRβ-expressing D4 cells with IC_{50} values generally less than those previously reported for **2** (Table 1).[42] Compounds **4** (N) and **6** (S) displayed 3- and 2-fold better activities respectively than the lead analog **2** in FRα-expressing RT16 cells. The impact of *N*-substitutions on compound **4** including **7** (N-CHO), **8** (N-$COCF_3$) and **9** (N-$COCH_3$) were disparate. Compound **8** showed comparable potency to **2** with RT16 cells, whereas **7** and **9** were much less inhibitory. The *N*-substituted compounds **7** (N-CHO), **8** (N-$COCF_3$), and **9** (N-$COCH_3$) showed activity in the rank order of **8** > **7** > **9** for FRα (RT16). Compounds **4**, **5** and **6**, were highly active (6-, 2-, and 16-fold, respectively) toward D4 cells (expresses FRβ) compared to compound **2**. For the *N*-substituted compounds with D4

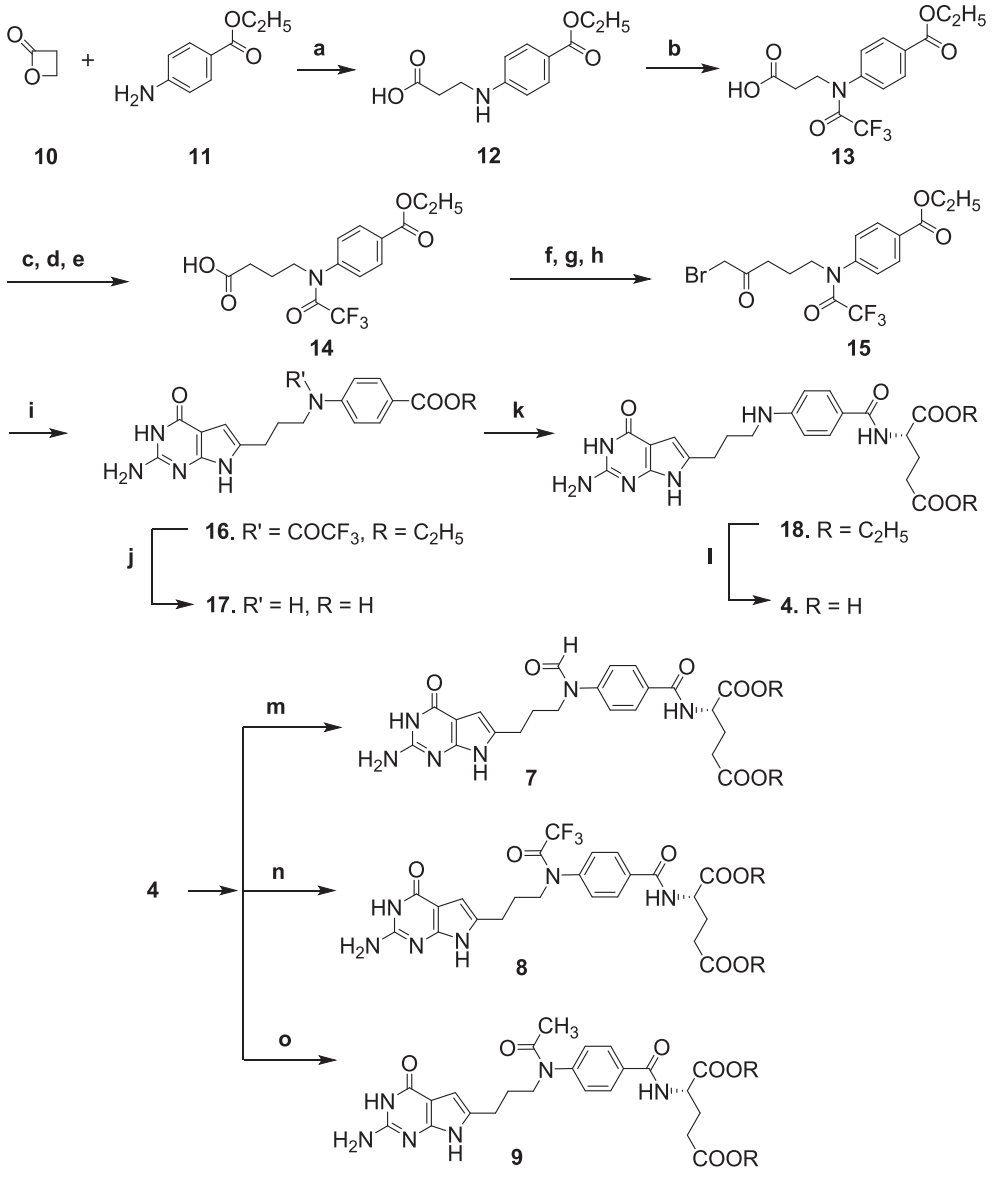

Scheme 1. . Reagents and conditions; (a) acetone, 4 h, reflux, 52%; (b) $(CF_3CO)_2O$, CH_2Cl_2, 2 h, rt, 88%; (c) oxalyl chloride, CH_2Cl_2, reflux, 1 h; (d) diazomethane, $(CH_3CH_2)_2O$, rt, 1 h; (e) $AgCOOCH_3$, water, 1–4 dioxane, 1.5 h, reflux, 38%; (f) oxalyl chloride, CH_2Cl_2, reflux, 1 h; (g) diazomethane, $(CH_3CH_2)_2O$, rt, 1 h; (h) 48% HBr in water, reflux, 1 h; (i) 2,6-diaminopyrimidin-4(3*H*)-one, DMF, rt, 3 d, 34%; (j) 1 N NaOH, rt, 12 h, 88%;(k) *N*-methylmorpholine 2-chloro-4, 6-methoxy-1,3,5-triarzine, L-glutamate dimethyl ester, *N*-methyl morpholine, DMF, 12 h, 43%; (l) 1 N NaOH, rt, 4 h, 88%; (m) HCOOH, $(CH_3CO)_2O$, reflux, 2 h, 42%; (n) $(CF_3CO)_2O$, 12 h, rt, 68%; (o) $(CH_3CO)_2O$, 12 h, rt, 74%.

cells, activity was comparable to (**9**) or exceeded (~16-fold for **7**; ~3-fold for **8**) that for **2**.

Relative inhibition by the heteroatom compounds toward KB human tumor cells generally paralleled that in FRα-expressing RT16 cells. Compounds **4** (N) and **6** (S) exhibited sub-nanomolar potencies (IC_{50} = 0.95 and 0.30 nM, respectively) in KB tumor cells which were ~2- and ~6-fold, respectively, greater than for the lead compound **2**.

From the results with the engineered CHO sublines, compounds **4–9** were all more selective toward FRs compared to PCFT and RFC. Antiproliferative activities toward PCFT- (R2/PCFT4) and RFC- (PC43-10) expressing cells ranged from modest to undetectable and were similar to those for compound **2**. These results contrast with those for the classic antifolates (MTX, PMX) which inhibit cells regardless of the expressed transporter (Table 1).

We previously reported that compound **2** was an inhibitor of *de novo* purine biosynthesis at the reaction catalyzed by GARFTase.[42] We evaluated inhibition of *de novo* purine biosynthesis by compounds **4–9** by comparing the extent of growth of KB cells in the presence of adenosine (60 μM) to that with thymidine (10 μM).[35,42] We also evaluated the protective effects of glycine (130 μM) to assess the potential for inhibition of C1 metabolism in mitochondria.[51] Results for the nucleoside/glycine protection experiments are shown in Fig. 7.

Adenosine completely reversed the drug effects of all the compounds, whereas thymidine and glycine were ineffective alone and they did not augment the effects of adenosine in combination (not shown). Thus, *de novo* purine biosynthesis rather than thymidylate synthase or mitochondrial C1 metabolism is the targeted pathway for compounds **4–9**. AICA (320 μM) has been used to identify GARFTase inhibitors as this is metabolized to AICA ribonucleotide (ZMP) to circumvent the GARFTase step.[35,42] As AICA was completely protective for compounds **4–9**, we conclude that GARFTase is the primary cellular target for this series.

5. Summary

In this report, we identified novel heteroatom substituted pyrrolo [2,3–*d*]pyrimidine compounds with N, O, or S replacements for CH_2 at position-11. Our results document remarkably increased in vitro antiproliferative activity resulting from heteroatom bridge substitutions toward CHO cell lines engineered to express human FRα or FRβ, and FRα-expressing human tumor cells, over the corresponding CH_2 analog **2**. All these compounds have substantial selectivities toward FRα and FRβ compared to RFC. PCFT-targeted activity for this series was modest. All compounds inhibited *de novo* purine biosynthesis, most

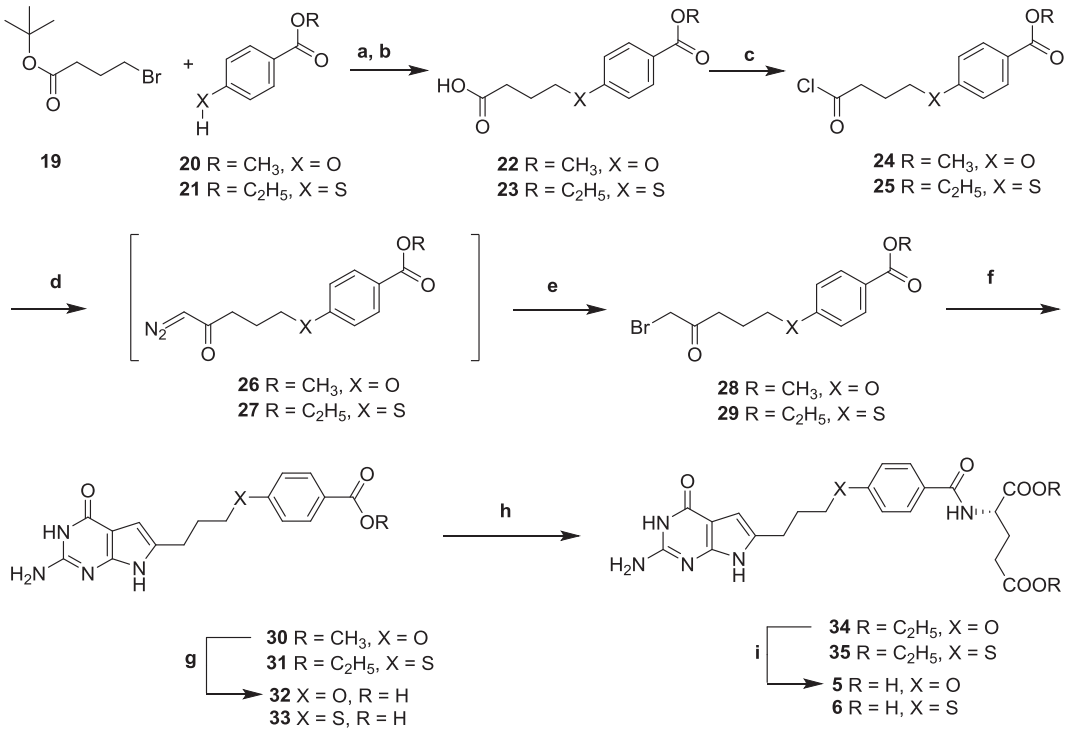

Scheme 2. . Reagent and conditions; (a) Cs_2CO_3, tetrabutyl ammonium chloride, DMF, 1 h, 100 °C, 47–65%; (b) CF_3COOH, CH_2Cl_2, 84–86%; (c) oxalyl chloride, CH_2Cl_2, reflux, 1 h, 79%; (d) diazomethane, $(CH_3CH_2)_2O$, rt, 1 h; (e) 48% HBr in water, 80 °C, 2 h, 86–94% (crude yield); (f) 2,6-diaminopyrimidin-4(3*H*)-one, DMF, rt, 3 d, 31–34%; (g) 1 N NaOH, rt, 12 h, 66–88%; (h) *N*-methylmorpholine 2-chloro-4, 6-methoxy-1,3,5-triarzine, L-glutamate diethyl ester, DMF, 12 h, 43–45%; (i) 1 N NaOH, rt, 4 h, 85–88%.

likely at GARFTase. Compounds **6** and **7** displayed ~16-fold increased activity over the CH_2 analog (**2**) and selectivity for FRβ compared to FRα, along with 6-fold increased activity against KB tumor cells for **6** over **2**. In addition to tumor targeting, these results suggest potential applications for targeting FRβ expressing hematopoietic cancers and activated macrophages.[5,20] As such, dual therapeutic targeting FRα-expressing tumors (e.g., epithelial ovarian cancer), along with FRβ-expressing tumor-associated macrophages, would be highly impactful. Collectively, these compounds provide an exciting platform for continued discovery of new and highly selective FR-targeted therapeutics for cancer, as well as other diseases.

6. Experimental section

A rotary evaporator was used to carry out evaporation in vacuo. Final compounds and intermediates were dried in a CHEM-DRY drying apparatus over P_2O_5 at 80 °C. A MEL-TEMP II melting point with a FLUKE 51 K/J electronic thermometer apparatus was used and uncorrected to record melting points. A Bruker WH-400 [400-megahertz (MHz)] spectrometer or a Bruker WH-500 (500 MHz) spectrometer was used to record proton nuclear magnetic resonance spectra (^{1}H NMR). Tetramethylsilane was used as an internal standard to express the chemical shift in ppm (parts per million): s, singlet; d, doublet; t, triplet; q, quartet; quin, quintet m, multiplet; and bs, broad singlet. Chemical names follow International Union of Pure and Applied Chemistry (IUPAC) nomenclature. Whatman Sil G/UV254 silica gel plates with a fluorescent indicator were used for performing thin-layer chromatography (TLC), and the spots were visualized under 254 and 365 nm illumination. All analytical samples were homogeneous on TLC in three different solvent systems. Solvents used for TLC were measured in volume. Columns of silica gel (230–400 mesh) (Fisher, Somerville, NJ) were used for chromatography. In spite of 24–48 h of drying in vacuo, fractional moles of water found in the analytical samples of antifolates could not be prevented and were confirmed by their presence in the ^{1}H NMR spectra. Chemicals and solvents were purchased from Aldrich Chemical Co. or Fisher Scientific Co. and were used as received. Elemental analysis (C, H, N, F, and S) was performed by Atlantic Microlab, Inc. (Norcross, GA). Element compositions were within 0.4% of the calculated values and confirmed > 95% purity for all the compounds submitted for biological evaluation.

6.1. Synthesis

3-((4-(ethoxycarbonyl)phenyl)amino)propanoic acid (12). A mixture of ethyl *p*-aminobenzoate (**11**) (1.65 g, 10 mmol) and β-propiolactone (**10**) (0.72 g, 10 mmol) in 15 mL of acetone was refluxed for 4 h. After evaporation of the solvent under reduced pressure, MeOH (10 mL) was added, followed by silica gel (5 g). The resulting plug was loaded on to a silica gel column and eluted with ethyl acetate: hexane 1:10. Fractions with R_f = 0.34 (hexane: EtOAc 1:1) were pooled and evaporated to afford **12** as yellow semisolid (1.23 g, yield; 52%). TLC R_f = 0.34 (1:1 hexane:EtOAc); ^{1}H NMR ($CDCl_3$) δ 1.26–1.29 (t, 3H, $OCH_2\underline{CH_3}$, J = 7 Hz), 2.51–2. 2.53 (t, 2H, $\underline{CH_2}CH_2NH$, J = 6.8 Hz), 3.30–3.32 (m, 2H, $CH_2\underline{CH_2}NH$), 4.18–4.24 (q, 2H, $O\underline{CH_2}CH_3$, J = 7 Hz), 6.59–6.61 (d, 2H, Ar-CH, J = 7.2 Hz), 7.68–7.70 (d, 2H, Ar-CH, J = 7.2 Hz).

3-(*N*-(4-(ethoxycarbonyl)phenyl)-2,2,2-trifluoroacetamido) propanoic acid (13). A solution of compound **12** (1.18 g, 5 mmol) in anhydrous CH_2Cl_2 (20 mL) was treated with triethylamine (1 mL) and trifluoroacetic anhydride (5 mL) under the anhydrous condition for 2 h. After removal of the excess of solvent under reduced pressure at 40–45 °C, the yellowish oily residue was dissolved in dichloromethane (20 mL) followed by silica gel (3 g). The resulting plug was loaded on to a silica gel column and eluted with 10% ethyl acetate in hexane. Fractions with and R_f = 0.59 (1:1 hexane: EtOAc) were pooled and evaporated to afford **13** (1.47 g, yield; 88%) as yellow semisolid. TLC R_f = 0.59 (1:1 hexane:EtOAc); ^{1}H NMR ($CDCl_3$) δ 1.40–1.44 (t, 3H, $OCH_2\underline{CH_3}$, J = 7.2 Hz), 2.68–2.72 (t, 2H, $\underline{CH_2}CH_2NCOCF_3$, J = 7.2 Hz),

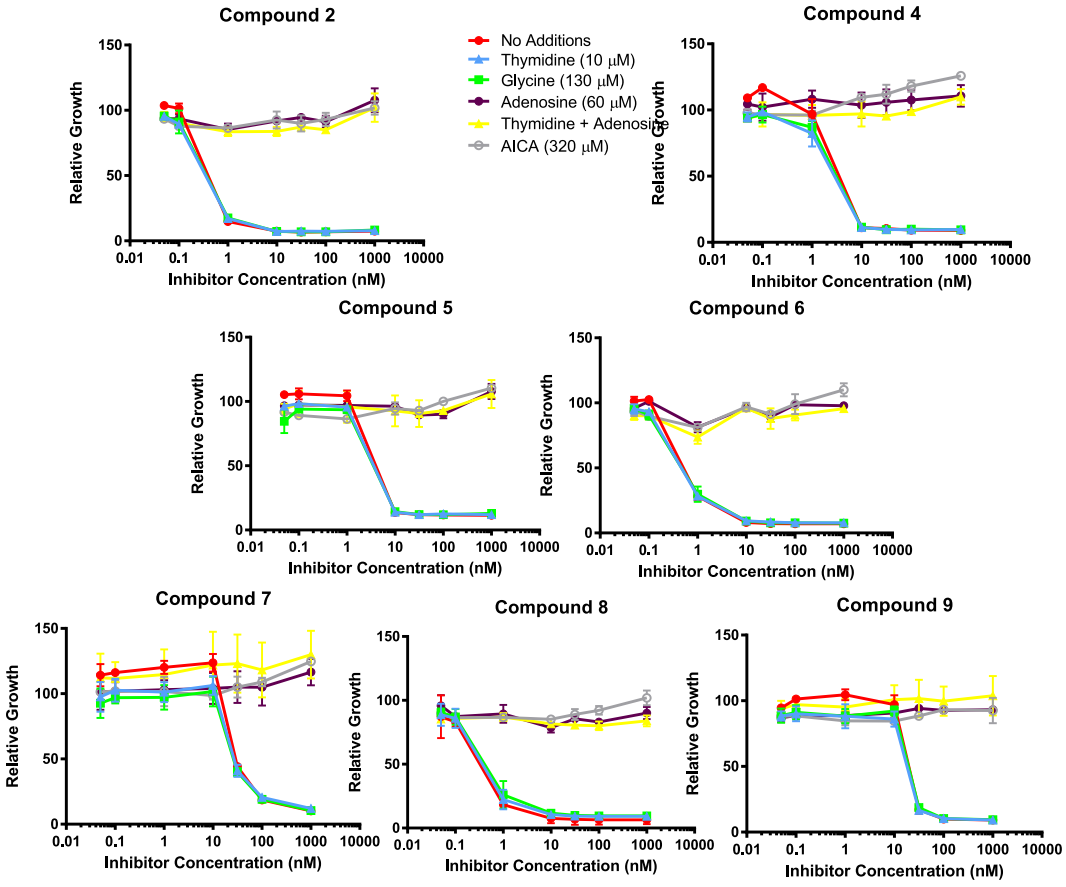

Fig. 7. Identification of the intracellular target by protection by nucleosides, glycine and AICA. KB cells were incubated with drugs in folate-, nucleoside-, and glycine-free RPMI 1640 medium with 10% dialyzed fetal bovine serum (FBS), antibiotics, L-glutamine, and 2 nM leucovorin (LCV) with a range of drug concentrations in the presence of folic acid (200 nM), adenosine (60 μM), thymidine (10 μM), glycine (130 μM) or AICA (320 μM). Cell proliferation was assayed with Cell Titer Blue™ (Promega) using a fluorescence plate reader[42]. Data are mean values for at least triplicate experiments. Error bars represent standard errors. Experimental details are summarized in the Experimental Section.

4.07–4.10 (t, 2H, $CH_2\underline{CH_2}NCOCF_3$, J = 7.2 Hz), 4.39–4.44 (q, 2H, $O\underline{CH_2}CH_3$, J = 7.2 Hz), 7.33–7.35 (d, 2H, Ar-CH, J = 8.4 Hz), 8.13–8.15 (d, 2H, CH_2, Ar-CH, J = 8.4 Hz). Anal. calcd ($C_{14}H_{14}F_3NO_5$): C, 50.46; H, 4.23; N, 4.20; F, 17.10. Found: C, 50.50; H, 4.22; N, 4.19; F, 16.87.

4-(*N*-(4-(ethoxycarbonyl)phenyl)-2,2,2-trifluoroacetamido)butanoic acid (14). Compound **13** (1.33 g, 4 mmol) was dissolved in 20 mL anhydrous dichloromethane and oxalyl chloride (2 mL, 23.30 mmol) was added. The resulting solution was refluxed for 1 h and then cooled to room temperature. After evaporating the solvent under reduced pressure, the residue was dissolved in 20 mL of diethyl ether. The resulting solution was added dropwise to ice-cooled diazomethane (generated in situ from 10 g of Diazald® by using Aldrich mini Diazald® Apparatus) in an ice bath over 10 min. The resulting mixture was allowed to stand for 30 min and then stirred for an additional 1 h, excess diazomethane was decomposed with l mL of acetic acid, and the solution evaporated to dryness to afford diazo compound. To a stirred suspension of silver acetate (1.2 g) in 30 mL of water was added a solution of the diazo compound in 30 mL of 1,4-dioxane. The reaction mixture was heated to reflux for 1.5 h, and then 1.2 g of sodium carbonate was added. The solid obtained was filtered and extracted with chloroform (3 × 25 mL). The combined chloroform extract was dried (Na_2SO_4), filtered, and the solvent was evaporated under reduced pressure. The residue was recrystallized from ethyl acetate to afford **14** (527 mg, yield over three steps 38%) as yellow semi-solid. TLC R_f = 0.64 (1:1 hexane:EtOAc); ^{1}H NMR ($CDCl_3$) δ 1.41–1.44 (t, 3H, $OCH_2\underline{CH_3}$, J = 7.2 Hz), 1.89–1.96 (quin, 2H, $CH_2\underline{CH_2}CH_2NCOCF_3$, J = 7.2 Hz), 2.42–2.46 (t, 2H, $\underline{CH_2}CH_2CH_2NCOCF_3$, J = 7.2 Hz), 3.82–3.86 (t, 2H, $CH_2CH_2\underline{CH_2}NCOCF_3$, J = 7.2 Hz), 4.40–4.45 (q, 2H, $O\underline{CH_2}CH_3$, J = 7.2 Hz), 7.31–7.34 (d, 2H, Ar-CH, J = 8.4 Hz), 8.14–8.16 (d, 2H, CH_2, Ar-CH, J = 8.4 Hz). Anal. calcd ($C_{15}H_{16}NF_3O_5$): C, 51.88; H, 4.64; N, 4.03; F, 16.41. Found: C, 51.82; H, 4.83; N, 3.99; F, 16.26.

4-((3-(2-amino-4-oxo-4,7-dihydro-3H-pyrrolo[2,3–*d*]pyrimidin-6-yl)propyl)amino) benzoic acid (17). To **14** (2.4 g, 10 mmol) in a 250 mL flask was added oxalyl chloride (5.14 mL, 60 mmol) and anhydrous CH_2Cl_2 (20 mL). The resulting solution was refluxed for 1 h and then cooled to room temperature. After the solvent was evaporated under reduced pressure, the residue was dissolved in 20 mL of diethyl ether. The resulting solution was added dropwise to ice-cooled diazomethane (generated in situ from 15 g of Diazald® by using Aldrich Mini Diazald® apparatus) in an ice bath over 10 min. The resulting mixture was allowed to stand for 30 min and then stirred for an additional 1 h. To this solution was added 48% HBr in water (20 mL). The resulting mixture was refluxed for 1.5 h. After the mixture was cooled to room temperature, the organic layer was separated, and the aqueous layer was extracted with Et_2O (2 × 200 mL). The combined organic layer and Et_2O extract was washed with two portions of 10% Na_2CO_3 solution and dried over Na_2SO_4. Evaporation of the solvent afforded **15** in 94% yield. To a suspension of 2,6-diaminopyrimidin-4-one (1.26 g, 10 mmol) in anhydrous DMF (25 mL) was added **15** (9.4 mmol). The resulting mixture was stirred under N_2 at room temperature for 3 days. After evaporation of the solvent under reduced pressure, MeOH (20 mL) was added followed by silica gel (5 g). The resulting plug was loaded on to a silica gel column and eluted with $CHCl_3$ followed by 3% MeOH in $CHCl_3$ and then 5% MeOH in $CHCl_3$. Fractions with and R_f = 0.58

(TLC) ($CHCl_3$:CH_3OH, 5:1) were pooled and evaporated to afford **16** (1.03 g, yield; 25%). Compound **16** (0.7 mmol) was dissolved in MeOH (10 mL) added 1 N NaOH (10 mL) and the mixture was stirred under N_2 at room temperature for 10 h. TLC showed the disappearance of the starting material and one major spot at the origin ($CHCl_3$: CH_3OH, 5:1). The reaction mixture was dissolved in water (10 mL), the resulting solution was cooled in an ice bath, and the pH was adjusted to 3–4 with the dropwise addition of 1 N HCl. The resulting suspension was frozen in the dry ice-acetone bath, thawed to 4–5 °C in the refrigerator, and filtered. The residue was washed with a small amount of cold water and dried in vacuum using P_2O_5 to afford the target compound **17** (196 mg, yield 86%) as yellow solid. TLC R_f = 0.19 (5:1 $CHCl_3$:MeOH); mp 154 °C, ^{1}H NMR (DMSO-d_6) δ 1.81–1.88 (quin, 2H, $CH_2\underline{CH_2}CH_2NH$, J = 7.2 Hz), 2.56–2.59 (t, $\underline{CH_2}CH_2CH_2NH$, CH_2, J = 7.2 Hz), 3.05–3.09 (m, 2H, $CH_2CH_2\underline{CH_2}NH$), 5.91 (s, 1H, C5-CH), 6.18 (bs, 2H, 2-NH_2, exch.), 6.54–6.56 (bd, 3H, Ar-CH and NH, J = 8.4 Hz, one proton exch), 7.64–7.66 (d, 2H, CH_2, Ar-CH, J = 8.4 Hz), 10.34 (s, 1H, 3-NH, exch.), 10.90 (s, 1H, 7-NH, exch.). Anal. calcd ($C_{16}H_{17}N_5O_3$·0.4 HCl): C, 56.20; H, 5.13; N, 20.48. Found: C, 56.39; H, 5.27; N, 20.41.

(4-((3-(2-amino-4-oxo-4,7-dihydro-3H-pyrrolo[2,3–*d*]**pyrimidin-6-yl)propyl)amino) benzoyl)-L-glutamic acid (4).** To a 250 mL round bottom flask, was added a mixture of compound **17** (100 mg, 0.2 mmol), *N*-methylmorpholine (0.4 mmol), 2-chloro-4,6-dimethoxy-1,3,5-triazine (0.4 mmol) and anhydrous DMF (7 mL). The resulting mixture was stirred at room temperature under the anhydrous condition for 1.5 h. *N*-mehtylmorpholine (0.64 mmol) and L-glutamate diethyl hydrochloride (0.3 mmol) were added in the reaction mixture. The resulting mixture was then stirred at room temperature under the anhydrous condition for 12 h. After evaporation of the solvent under reduced pressure, MeOH (20 mL) was added followed by silica gel (1 g). The resulting plug was loaded on to a silica gel column and eluted with $CHCl_3$ followed by 3% MeOH in $CHCl_3$ and then with 5% MeOH in $CHCl_3$. Fractions with R_f = 0.45 ($CHCl_3$:CH_3OH, 5:1) were pooled and evaporated to afford **18** (96 mg, yield 61%) as solid. Compound **18** (0.15 mmol) was dissolved in MeOH (10 mL) added 1 N NaOH (10 mL) and the mixture was stirred under N_2 at room temperature for 10 h. TLC showed the disappearance of the starting material and one major spot at the origin ($CHCl_3$: CH_3OH, 5:1). The reaction mixture was dissolved in water (10 mL), the resulting solution was cooled in an ice bath, and the pH was adjusted to 3–4 with dropwise addition of 1 N HCl and acetic acid. The resulting suspension was frozen in the dry ice-acetone bath, thawed to 4–5 °C in the refrigerator, and filtered. The residue was washed with a small amount of cold water and dried in vacuum using P_2O_5 to afford the target compound **4** (58 mg, yield 84%) as a yellow powder. TLC R_f = 0.16 (5:1 $CHCl_3$:MeOH); mp 163 °C; ^{1}H NMR (DMSO-d_6) δ 1.92–1.95 (quin, 2H, $CH_2\underline{CH_2}CH_2NH$, J = 7.2 Hz), 1.97–2.09 (m, 2H, β -CH_2), 2.32–2.35 (t, 2H, γ-CH_2, J = 7.5 Hz), 2.58–2.61 (t, 2H, $\underline{CH_2}CH_2CH_2NH$, J = 7.2 Hz), 3.31–3.34 (m, 2H, $CH_2CH_2\underline{CH_2}NH$), 4.34–4.37 (m, 1H, α-CH), 5.91–5.91 (d, 1H, Ar-CH, J = 2 Hz), 5.97 (bs, 2H, 2-NH_2, exch.), 6.22–6.24 (t, 1H, $CH_2CH_2CH_2\underline{NH}$, J = 5.5 Hz, exch.), 6.55–6.56 (d, 2H, Ar-CH, J = 9 Hz), 7.65–7.67 (d, 2H, Ar-CH, J = 9 Hz), 8.09–8.10 (d, 1H, NH, J = 7.5 Hz, exch.), 10.14 (s, 1H, 3-NH, exch.), 10.85 (s, 1H, 7-NH, exch.). Anal. calcd ($C_{21}H_{24}N_6O_6$·0.5H_2O0.5CH_3COOH): C, 53.33; H, 5.49; N, 16.96. Found: C, 53.27; H, 5.59; N, 16.61.

(4-(*N*-(3-(2-amino-4-oxo-4,7-dihydro-3*H*-pyrrolo [2,3-*d*] pyrimidin-6- yl)propyl)formamido) benzoyl)-L-glutamic acid (7). To a solution of **4** (110 mg, 0.25 mmol) in 97% formic acid (5 mL) was added acetic anhydride (1 mL), and the reaction mixture was stirred at 25 °C for 3 h. The solvent was removed under reduced pressure and the residue dissolved in 1 N NaOH at 0 °C. The filtrate was acidified to pH 4 with 0.5 N HCl and stored at 0 °C for 2 h. The yellow solid was collected by filtration and dried over P_2O_5 to give 40 mg (yield 35%) of **7**. TLC R_f = 0.19 (5:1 $CHCl_3$:MeOH); mp 153 °C; ^{1}H NMR (DMSO-d_6) δ 1.92–1.95 (quin, 2H, $CH_2\underline{CH_2}CH_2NCHO$, J = 7.2 Hz), 1.97–2.11 (m, 2H, β -CH_2), 2.35–2.38 (t, 2H, γ-CH_2, J = 7.5 Hz), 2.44–2.47 (t, 2H, $\underline{CH_2}CH_2CH_2NCHO$, J = 7.2 Hz), 3.84–3.88 (t, 2H, $CH_2CH_2\underline{CH_2}NCHO$, J = 7.5 Hz) 4.38–4.43 (m, 2H, α-CH), 5.85 (s, 1H, C5-CH), 5.97 (s, 2H, 2-NH_2, exch.), 7.45–7.78 (d, 1.72H, Ar-CH, J = 8.4 Hz, rotamer of formamide), 7.51–7.53 (d, 0.28H, Ar-CH, J = 8.4 Hz, rotamer of formamide), 7.91–7.95 (d, 2H, Ar-CH, J = 8.4 Hz), 8.64–8.66 (d, 1H, Ar-CO$\underline{NH}$, J = 7.6 Hz, exch.), 10.23 (bs, H, 3-NH, exch.), 10.93 (s, H, 7-NH, exch.). Anal. calcd ($C_{22}H_{24}N_6O_7$·1.5H_2O2.5 HCl): C, 45.25; H, 5.25; N, 13.47. Found: C, 45.56; H, 4.89; N, 13.40.

(4-(*N*-(3-(2-amino-4-oxo-4,7-dihydro-3*H*-pyrrolo [2,3-*d*] pyrimidin-6-yl)propyl)-2,2,2-trifluoroacetamido)benzoyl)-L-glutamic acid (8). 5 mL trifluoroacetic anhydride was added to a solution of **4** (110 mg, 0.25 mmol) in 10 mL dichloromethane, and the reaction mixture was stirred at 25 °C for 3 h. The solvent was removed under reduced pressure and the residue was suspended in water. 1 N NaOH was added dropwise to the suspension and pH was adjusted to 4. The suspension was stored at 0 °C for 2 h. The yellow solid was collected by filtration and dried over P_2O_5 to give 83 mg (yield 76%) of **8**. TLC R_f = 0.21 (5:1 $CHCl_3$:MeOH); mp 158 °C; ^{1}H NMR (DMSO-d_6) δ 1.87–2.11 (m, 4H, $CH_2\underline{CH_2}CH_2NCOCF_3$ and β -CH_2), 2.33–2.37 (t, 2H, γ-CH_2, J = 7.5 Hz), 2.62–2.66 (t, 2H, $\underline{CH_2}CH_2CH_2NCOCF_3$, J = 7.2 Hz), 3.97–3.99 (t, 2H, $CH_2CH_2\underline{CH_2}NCOCF_3$, J = 7.2 Hz), 4.38–4.44 (m, 1H, α-CH), 5.92 (s, 1H, C5-CH), 5.97 (bs, 2H, 2-NH_2, exch.), 7.40–7.42 (d, 2H, Ar-CH, J = 8 Hz), 7.94–7.96 (d, 2H, Ar-CH, J = 8 Hz), 8.76–8.78 (d, 1H, Ar-CO$\underline{NH}$, J = 8 Hz, exch.), 10.39 (bs, H, 3-NH, exch.), 10.99 (s, H, 7-NH, exch.). Anal. calcd ($C_{23}H_{13}N_6O_7F_3$·0.5H_2O): C, 49.20; H, 4.31; N, 14.97; F, 10.15. Found: C, 49.16; H, 4.52; N, 15.05; F, 9.82.

(4-(*N*-(3-(2-amino-4-oxo-4,7-dihydro-3*H*-pyrrolo [2,3-*d*] pyrimidin-6-yl)propyl)acetamido)benzoyl)-L-glutamic acid (9). Compound **4** (110 mg, 0.25 mmol) was added in 5 mL acetic anhydride, and the reaction mixture was stirred under the anhydrous condition at 25 °C for 3 h. The excess of acetic anhydride was removed under reduced pressure. The residue was suspended in cold water and basified using 1 N NaOH. The suspension was then filtered and acidified to pH 4 with 0.5 N HCI and stored at 0 °C for 2 h. The white solid was collected by filtration and dried over P_2O_5 to give 57 mg (yield 47%) of **9**. TLC R_f = 0.19 (5:1 $CHCl_3$:MeOH); mp 166 °C; ^{1}H NMR (DMSO-d_6) δ 1.93–2.14 (m, 4H, $CH_2\underline{CH_2}CH_2NCOCH_3$, β -CH_2), 2.05 (s, 3H, $CH_2CH_2CH_2NCO\underline{CH_3}$), 2.35–2.39 (t, 2H, γ-CH_2, J = 7.5 Hz), 2.64–2.67 (t, 2H, $\underline{CH_2}CH_2CH_2NCOCH_3$, J = 8 Hz), 3.89–3.92 (t, 2H, $CH_2CH_2\underline{CH_2}NCOCH_3$, J = 8 Hz), 4.38–4.44 (m, 1H, α-CH), 5.91 (s, 1H, C5-CH), 5.99 (s, 2H, 2-NH_2, exch.), 7.34–7.36 (d, 2H, Ar-CH, J = 8 Hz), 7.93–7.95 (d, 2H, Ar-CH, J = 8 Hz), 8.68–8.70 (d, 1H, Ar-CO$\underline{NH}$, J = 8 Hz, exch.), 10.16 (bs, H, 3-NH, exch.), 10.83 (s, H, 7-NH, exch.), 12.45 (bs, 2H, 2COOH, exch.). Anal. calcd ($C_{23}H_{26}N_6O_7$·0.5 H_2O·1.6HCl): C, 49.27; H, 5.21; N, 14.67. Found: C, 48.99; H, 4.99; N, 15.37.

4-(4-(ethoxycarbonyl)phenoxy)butanoic acid (22). To 100 mL rbf was added a mixture of compound **20** (1.66 g, 10 mmol), cesium carbonate (3.26 g, 10 mmol), TBAI (3.70 g, 10 mmol) and anhydrous DMF (20 mL). Compound **19** (2.23 g, 10 mmol) was added dropwise to the mixture. The reaction mixture was then stirred at room temperature for 3 h. Ethyl acetate was added into the reaction mixture. The combined mixture was washed with two portions of water. After evaporation of the solvent under reduced pressure MeOH (20 mL) was added followed by silica gel (1 g). The resulting plug was loaded on to a silica gel column and eluted with 1:10 (ethyl acetate: hexane). Fractions with and R_f = 0.64 (hexane:ethyl acetate 1:1) were pooled and evaporated to afford tert-butyl esters (1.47 g, yield; 47%). Trifluoroacetic acid was then added into the tert-butyl esters and mixture was stirred at room temperature for 30 min. Excess of trifluoroacetic acid was evaporated and MeOH (20 mL) was added followed by silica gel (1 g). The resulting plug was loaded on to a silica gel column and eluted with 1:10 (ethyl acetate: hexane). Fractions with and R_f = 0.45 (TLC) (Hexane: ethylacetate, 1:1) were pooled and evaporated to afford **22** (1 g, yield 83%) as white solid. TLC R_f = 0.45 (1:1 hexane:EtOAc); mp 112 °C; ^{1}H NMR ($CDCl_3$) δ 2.13–2.20 (quin, 2H, $CH_2\underline{CH_2}CH_2O$, J = 7.2 Hz), 2.60–2.64

(t, 2H, $\underline{CH_2}CH_2CH_2O$, J = 7.2 Hz), 3.90 (s, 3H, $O\underline{CH_3}$), 4.08–4.11 (t, 2H, $CH_2CH_2\underline{CH_2}O$, J = 7.2 Hz), 6.91–6.93 (d, 2H, Ar-CH, J = 8.8 Hz), 7.99–8.01 (d, 2H, Ar-CH, J = 8.8 Hz).

4-((4-(ethoxycarbonyl)phenyl)thio)butanoic acid (23). Carboxylic acid **23** was synthesized from compound **21** using the synthetic procedure as for carboxylic acid **22** in 74% yield as white solid over two-step. TLC R_f = 0.52 (1:1 hexane:EtOAc); mp 76 °C; ^{1}H NMR ($CDCl_3$) δ 1.39–1.43 (t, 2H, $OCH_2\underline{CH_3}$, J = 7.2 Hz), 2.03–2.06 (quin, 2H, $CH_2\underline{CH_2}CH_2S$, J = 7.2 Hz), 2.53–2.60 (t, 2H, $\underline{CH_2}CH_2CH_2O$, J = 7.2 Hz), 3.07–3.10 (t, 2H, $CH_2CH_2\underline{CH_2}S$, J = 7.2 Hz), 4.36–4.41 (q, 2H, $O\underline{CH_2}CH_3$, J = 7.2 Hz), 7.33–7.35 (d, 2H, Ar-CH, J = 8.4 Hz), 7.95–7.97 (d, 2H, CH_2, Ar-CH, J = 8.4 Hz).

4-(3-(2-amino-4-oxo-4,7-dihydro-3*H*-pyrrolo [2,3-*d*] pyrimidin-6-yl)propoxy)benzoic acid (32). To **22** (2.52 g, 10 mmol) in a 250 mL flask was added oxalyl chloride (5.14 g, 60 mmol) and anhydrous CH_2Cl_2 (20 mL). The resulting solution was refluxed for 1 h and then cooled to room temperature. After the solvent was evaporated under reduced pressure, the residue was dissolved in 20 mL of Et_2O. The resulting solution was added dropwise to an ice-cooled diazomethane (generated in situ from 15 g of Diazald® by using Aldrich Mini Diazald® apparatus) in an ice bath over 10 min. The resulting mixture was allowed to stand for 30 min and then stirred for an additional 1 h. To this solution was added 48% HBr (20 mL). The resulting mixture was refluxed for 1.5 h. After the mixture was cooled to room temperature, the organic layer was separated, and the aqueous layer was extracted with Et_2O (2 × 200 mL). The combined organic layer and Et_2O extract was washed with two portions of 10% Na_2CO_3 solution and dried over Na_2SO_4. Evaporation of the solvent afforded **28** in 94% crude yield. To a suspension of 2,6-diaminopyrimidin-4-one (1.26 g, 10 mmol) in anhydrous DMF (25 mL) was added **28** (9.4 mmol). The resulting mixture was stirred under N_2 at room temperature for 3 days. After evaporation of the solvent under reduced pressure, MeOH (20 mL) was added followed by silica gel (5 g). The resulting plug was loaded on to a silica gel column and eluted with $CHCl_3$ followed by 3% MeOH in $CHCl_3$ and then 5% MeOH in $CHCl_3$. Fractions with and R_f = 0.48 (TLC) ($CHCl_3$:CH_3OH, 5:1) were pooled and evaporated to afford **30** (1 g, yield 31%). Compound **30** (1 g, 2.92 mmol) was dissolved in MeOH (10 mL) added 1 N NaOH (10 mL) and the mixture was stirred under N_2 at room temperature for 10 h. TLC showed the disappearance of the starting material and one major spot at the origin ($CHCl_3$: MeOH 5:1). The reaction mixture was dissolved in water (10 mL), the resulting solution was cooled in an ice bath, and the pH was adjusted to 3–4 with the dropwise addition of 1 N HCl. The resulting suspension was frozen in the dry ice-acetone bath, thawed to 4–5 °C in the refrigerator, and filtered. The residue was washed with a small amount of cold water and dried in vacuum using P_2O_5 to afford the compound **32** (638 mg, yield 66%) as white solid. TLC R_f = 0.15 (5:1 $CHCl_3$:MeOH); mp 155 °C; ^{1}H NMR (DMSO-d_6) δ 2.02–2.07 (quin, 2H, $CH_2\underline{CH_2}CH_2O$, J = 7.2 Hz), 2.63–2.69 (t, 2H, $\underline{CH_2}CH_2CH_2O$, J = 7.2 Hz), 4.03–4.06 (t, 2H, $CH_2CH_2\underline{CH_2}O$, J = 7.2 Hz), 5.95 (s, 1H, C5-CH), 6.60 (bs, 2H, 2-NH_2, exch.), 6.99–7.02 (d, 2H, Ar-CH, J = 8.8 Hz), 7.86–7.89 (d, 2H, Ar-CH, J = 8.8 Hz), 10.67 (s, 1H, 3-NH, exch.), 11.18 (s, 1H, 7-NH, exch.).

4-((3-(2-amino-4-oxo-4,7-dihydro-3*H*-pyrrolo [2,3-*d*] pyrimidin-6-yl)propyl)thio)benzoic acid (33). Carboxylic acid **33** was synthesized from compound **23** using the synthetic procedure as for carboxylic acid **32** from compound **22** in 22% yield as white solid over five steps. TLC R_f = 0.22 (1:1 hexane:EtOAc); mp 143 °C; ^{1}H NMR (DMSO-d_6) δ 1.89–1.96 (quin, 2H, $CH_2\underline{CH_2}CH_2S$, J = 7.2 Hz), 2.64–2.67 (t, 2H, $\underline{CH_2}CH_2CH_2S$, J = 7.2 Hz), 3.03–3.07 (t, 2H, $CH_2CH_2\underline{CH_2}S$, J = 7.2 Hz), 5.95 (s, 1H, C5-CH), 6.02 (bs, 2H, 2-NH_2, exch.), 7.34–7.36 (d, 2H, Ar-CH, J = 8.8 Hz), 7.82–7.84 (d, 2H, Ar-CH, J = 8.8 Hz), 10.47 (s, 1H, 3-NH, exch.), 11.06 (s, 1H, 7-NH, exch.).

(4-(3-(2-amino-4-oxo-4,7-dihydro-3H-pyrrolo [2,3-*d*] pyrimidin-6-yl)propoxy)benzoyl)-L-glutamic acid (5). To a 250 mL rbf, was added a mixture of compound **32** (80 mg, 0.24 mmol), *N*-methylmorpholine (0.48 mmol), 2-chloro-4,6-dimethoxy-1,3,5-triazine (0.48 mmol) and anhydrous DMF (10 mL). The resulting mixture was stirred at room temperature under the anhydrous condition for 1.5 h. *N*-mehtylmorpholine (0.48 mmol) and L-glutamate di-*tert*-butyl hydrochloride (0.36 mmol) were added in reaction mixture. The resulting mixture was then stirred at room temperature under the anhydrous condition for 12 h. After evaporation of the solvent under reduced pressure, MeOH (20 mL) was added followed by silica gel (1 g). The resulting plug was loaded on to a silica gel column and eluted with $CHCl_3$ followed by 1% MeOH in $CHCl_3$. Fractions with R_f = 0.52 ($CHCl_3$:CH_3OH, 5:1) were pooled and evaporated to afford **34** (56 mg, yield 45%) as solid. Compound **34** (56 mg, 0.11 mmol) was dissolved in MeOH (10 mL) added 1 N NaOH (10 mL) and the mixture was stirred under N_2 at room temperature for 10 h. TLC showed the disappearance of the starting material and one major spot at the origin ($CHCl_3$: MeOH 5:1). The reaction mixture was dissolved in water (10 mL), the resulting solution was cooled in an ice bath, and the pH was adjusted to 3–4 with the dropwise addition of 1 N HCl. The resulting suspension was frozen in the dry ice-acetone bath, thawed to 4–5 °C in the refrigerator, and filtered. The residue was washed with a small amount of cold water and dried in vacuum using P_2O_5 to afford the target compound **(5)** (34 mg, yield 68%) as white powder. TLC R_f = 0.12 (5:1 $CHCl_3$:MeOH); mp 173 °C; ^{1}H NMR (DMSO-d_6) δ 1.91–2.09 (m, 4H, $CH_2\underline{CH_2}CH_2O$ and β-CH_2), 2.33–2.37 (t, 2H, γ-CH_2, J = 7.6 Hz), 2.45–2.68 (t, 2H, $\underline{CH_2}CH_2CH_2O$, J = 7.6 Hz), 4.03–4.06 (t, 2H, $CH_2CH_2\underline{CH_2}O$, J = 7.6 Hz), 4.35–4.40 (m, 1H, α-CH), 5.90 (s, 1H, C5-CH), 5.99 (bs, 2H, 2-NH_2, exch.), 6.99–7.02 (d, 2H, CH_2, Ar-CH, J = 8.8 Hz), 7.84–7.87 (d, 2H, Ar-CH, J = 8.8 Hz), 8.44–8.46 (d, 1H, Ar-CO$\underline{NH}$, J = 7.5 Hz, exch.), 10.16 (s, 1H, 3-NH, exch.), 10.89 (s, 1H, 7-NH, exch.). Anal. calcd ($C_{21}H_{23}N_5O_7 \cdot 2\ H_2O$): C, 51.11; H, 5.51; N, 14.19: Found: C, 50.94; H, 5.45; N, 14.00.

(4-((3-(2-amino-4-oxo-4,7-dihydro-3*H*-pyrrolo [2,3-*d*] pyrimidin-6-yl)propyl)thio)benzoyl)-L-glutamic acid (6). Target compound **6** was synthesized from compound **33** using the synthetic procedure as for target compound **5** from compound **32** in 38% yield as buff color solid over two steps. TLC R_f = 0.14 (5:1 $CHCl_3$:MeOH); mp 171 °C; ^{1}H NMR (DMSO-d_6) δ 1.95–2.13 (m, 4H, $CH_2\underline{CH_2}CH_2S$ and β-CH_2), 2.33–2.37 (t, 2H, γ-CH_2, J = 7.2 Hz), 2.62–2.66 (t, 2H, $\underline{CH_2}CH_2CH_2S$, J = 7.2 Hz), 3.02–3.06 (t, 2H, $CH_2CH_2\underline{CH_2}S$, J = 7.2 Hz), 4.38–4.39 (m, 1H, α-CH), 5.89 (s, 1H, C5-CH), 5.99 (bs, 2H, 2-NH_2, exch.), 7.35–7.37 (d, 2H, Ar-CH, J = 8.4 Hz), 7.80–7.82 (d, 2H, Ar-CH, J = 8.4 Hz), 8.57–8.59 (d, 1H, Ar-CO$\underline{NH}$, J = 7.5 Hz, exch.), 10.16 (s, 1H, 3-NH, exch.), 10.88 (s, 1H, 7-NH, exch.). Anal. calcd ($C_{21}H_{23}N_5O_6S \cdot 0.5\ H_2O$): C, 52.27; H, 5.01; N, 14.51; S, 6.65. Found: C, 52.08; H, 4.86; N, 14.51; S, 6.47.

6.2. Molecular modeling and computational studies

All the compounds were docked on to the X-ray crystal structures of human FRα (PDB 5IZQ, 3.60 Å)[35,37,45], FRβ (PDB 4KN2, 2.6 Å)[23], and GARFTase (PDB 5J9F, 2.1 Å)[35,37] to analyze the potential binding modes, binding energies, and favorable or unfavorable interactions. The energy-minimized crystallized ligand **3**[35] and PMX were redocked with an RMSD (root-mean-square deviation) of 0.89 and 0.91 for the best-scored pose, thus validating the docking process. The crystal structure PDBs were obtained from the protein database. All docking procedures were performed using various modules of Schrödinger Maestro suite (Schrödinger, LLC, New York, NY, 2019).[44] The polypeptide structures of FRα, FRβ and GARFTase were optimized and prepared for docking using the Maestro Protein Preparation Wizard to assess bond order and missing hydrogens, followed by energy minimization using the OPLS3e force field. Gaps in the protein structures were not corrected as they were far from the active site. The Maestro induced-fit Grid Generation module was then used to define a 15 × 15 × 15 Å grid from the center of all the ligands. Ligands used in the computational docking study were built using the Maestro 2D Build module. The Maestro LigPrep module was then used to generate conformers of each compound

subjected to energy minimization using the OPLS3e force field protocol. The resulting compounds were docked into the prepared FRα, FRβ, and GARFTase structures using the Maestro Induced Fit Docking. Induced Fit Docking was performed with standard precision with flexible ligand sampling. A total of 20 initial poses were generated for each compound. Based on the pose score, the top 4 poses were selected and subjected to energy minimization using the OPLS3e force field. Finally, the top 2 poses per compound were generated and ranked according to Glide score, which is an approximation of binding energy defined by receptor-ligand complex energies. The top pose was analyzed and presented in the Biological Evaluation and Discussion. Docking scores are listed in Table 2S (supporting information).

6.3. Cell lines and assays of antitumor drug activities

The engineered CHO sublines including RFC-, PCFT-, and FRα-null MTXRIIOua^{R}2-4 (R2) and RFC- (PC43-10), PCFT- (R2/PCFT4), FRα- (RT16), and FRβ- (D4) expressing CHO sublines were previously described.[33,34,42,48–50] The CHO cells were grown in α-minimal essential medium (MEM) supplemented with 10% bovine calf serum (Invitrogen, Carlsbad, CA), L-glutamine (2 mM), penicillin (1000 U/mL), and streptomycin (1000 μg/mL) at 37 °C with 5% CO_2. R2 transfected cells (PC43-10, RT16, D4, R2/PCFT4) were cultured in complete α-MEM media plus G418 (1 mg/mL). Prior to the cell proliferation assays (see below), RT16 and D4 cells were cultured in complete folate-free RPMI 1640 (without added folate), plus 10% dialyzed fetal bovine serum (FBS) (Sigma-Aldrich) and penicillin/streptomycin for 3 days. Human KB carcinoma cells were purchased from ATCC (Manassas, VA) continuously maintained in complete folate-free (FF) RPMI with 10% fetal bovine serum and 1% penicillin-streptomycin and L-glutamine.

For growth inhibition studies, cells (CHO, KB) were plated in 96 well dishes (~2000 cells/well, total volume of 200 μL) and treated with a range of drug concentrations (0–1000 nM) in complete folate-free RPMI 1640 medium with 10% dialyzed FBS, supplemented with 2 nM (KB, RT16, D4 CHO cells) or 25 nM (PC43-10, R2/PCFT4) leucovorin, as described.[33–35,38–42,50] To confirm FR-mediated drug uptake, 200 nM folic acid was added to parallel incubations for KB, RT16 and D4 cells. After 96 h, viable cells were assayed with Cell-Titer Blue™ reagent (Promega, Madison, WI), and fluorescence was measured with a fluorescence plate reader. Fluorescence measurements were used for calculations of IC_{50} values, corresponding to the drug concentrations at which cells showed 50% loss of proliferation.

To confirm the targeted pathway or enzyme, in vitro growth inhibition of KB tumor cells was measured with complete folate- and glycine-free RPMI 1640 supplemented with 10% dialyzed fetal bovine serum in the presence of thymidine (10 μM), adenosine (60 μM) and/or glycine (130 μM).[33–35,38–42,50] For *de novo* purine biosynthesis inhibitors, additional protection experiments used AICA (320 μM) to distinguish inhibitory effects at GARFTase from those at AICARFTase.[33–35,38–42,50]

7. Statistical analysis

Descriptive statistical tests (e.g., t-tests) were conducted using GraphPad 6.0 software (La Jolla, CA).

Declaration of Competing Interest

The authors declare that they have no known competing financial interests or personal relationships that could have appeared to influence the work reported in this paper.

Acknowledgments

This work was supported in part by grants from the National Institutes of Health R01 CA53535 (LHM and ZH), R01 CA125153 (AG), R01 CA152316 (LHM and AG), and R01 CA166711 (AG and LHM), the Eunice and Milton Ring Endowed Chair for Cancer Research (LHM), and the Duquesne University Adrian Van Kaam Chair in Scholarly Excellence (AG). AD was supported by T32 CA009531 (LHM) and F30 CA228221 (AD).

Appendix A. Supplementary material

Supplementary data to this article can be found online at https://doi.org/10.1016/j.bmc.2020.115544.

References

1. Stokstad ELR. Historial perspective on key advances in the biochemistry and physiology of folates. In: Picciano MF, Stokstad ELR, Gregory JF, eds. *Contemporary Issues in Clinical Nutrition.* New York: Wiley-Liss; 1990:1–21. Folic Acid Metabolism in Heath and Disease.
2. Shuvalov O, Petukhov A, Daks A, Fedorova O, Vasileva E, Barlev NA. One-carbon metabolism and nucleotide biosynthesis as attractive targets for anticancer therapy. *Oncotarget.* 2017;8:23955–23977.
3. Hou Z, Matherly LH. Biology of the major facilitative folate transporters SLC19A1 and SLC46A1. *Curr Top Membr.* 2014;73:175–204.
4. Matherly LH, Hou Z, Deng Y. Human reduced folate carrier: translation of basic biology to cancer etiology and therapy. *Cancer Metastasis Rev.* 2007;26:111–128.
5. Elnakat H, Ratnam M. Distribution, functionality and gene regulation of folate receptor isoforms: implications in targeted therapy. *Adv Drug Deliv Rev.* 2004;56:1067–1084.
6. Matherly LH, Hou Z, Gangjee A. The promise and challenges of exploiting the proton-coupled folate transporter for selective therapeutic targeting of cancer. *Cancer Chemother Pharmacol.* 2018;81:1–15.
7. Zhao R, Goldman ID. The molecular identity and characterization of a Proton-coupled Folate Transporter–PCFT; biological ramifications and impact on the activity of pemetrexed. *Cancer Metastasis Rev.* 2007;26:129–139.
8. Desmoulin SK, Hou Z, Gangjee A, Matherly LH. The human proton-coupled folate transporter: Biology and therapeutic applications to cancer. *Cancer Biol Ther.* 2012;13:1355–1373.
9. Qiu A, Jansen M, Sakaris A, et al. Identification of an intestinal folate transporter and the molecular basis for hereditary folate malabsorption. *Cell.* 2006;127:917–928.
10. Inoue K, Nakai Y, Ueda S, et al. Functional characterization of PCFT/HCP1 as the molecular entity of the carrier-mediated intestinal folate transport system in the rat model. *Am J Physiol-Gastrointestinal LiverPhysiol.* 2008;294:G660–G668.
11. Chabner BA, Allegra CJ. *Cancer chemotherapy and biotherapy principles and practice: Antifolates.* 5 ed. Philadelphia; Baltimore; New York: Wolters Kluwer: Lippincott Williams & Wilkins; 2011:109–138.
12. Visentin M, Zhao R, Goldman ID. The antifolates. *Hematol Oncol Clin North Am.* 2012;26:629–648 ix.
13. Wessels JA, Huizinga TW, Guchelaar HJ. Recent insights in the pharmacological actions of methotrexate in the treatment of rheumatoid arthritis. *Rheumatology (Oxford).* 2008;47:249–255.
14. Chattopadhyay S, Moran RG, Goldman ID. Pemetrexed: biochemical and cellular pharmacology, mechanisms, and clinical applications. *Mol Cancer Ther.* 2007;6:404–417.
15. Gonen N, Assaraf YG. Antifolates in cancer therapy: structure, activity and mechanisms of drug resistance. *Drug Resist Updat.* 2012;15:183–210.
16. Gibbs DD, Theti DS, Wood N, et al. BGC 945, a novel tumor-selective thymidylate synthase inhibitor targeted to alpha-folate receptor-overexpressing tumors. *Cancer Res.* 2005;65:11721–11728.
17. Vergote IB, Marth C, Coleman RL. Role of the folate receptor in ovarian cancer treatment: evidence, mechanism, and clinical implications. *Cancer Metastasis Rev.* 2015;34:41–52.
18. Xia W, Low PS. Folate-targeted therapies for cancer. *J Med Chem.* 2010;53:6811–6824.
19. Parker N, Turk MJ, Westrick E, Lewis JD, Low PS, Leamon CP. Folate receptor expression in carcinomas and normal tissues determined by a quantitative radioligand binding assay. *Anal Biochem.* 2005;338:284–293.
20. Puig-Kroger A, Sierra-Filardi E, Dominguez-Soto A, et al. Folate receptor beta is expressed by tumor-associated macrophages and constitutes a marker for M2 anti-inflammatory/regulatory macrophages. *Cancer Res.* 2009;69:9395–9403.
21. Shen J, Hu Y, Putt KS, et al. Assessment of folate receptor alpha and beta expression in selection of lung and pancreatic cancer patients for receptor targeted therapies. *Oncotarget.* 2018;9:4485–4495.
22. Weitman SD, Weinberg AG, Coney LR, Zurawski VR, Jennings DS, Kamen BA. Cellular Localization of the Folate Receptor: Potential Role in Drug Toxicity and Folate Homeostasis. *Cancer Res.* 1992;52:6708–6711.
23. Wibowo AS, Singh M, Reeder KM, et al. Structures of human folate receptors reveal biological trafficking states and diversity in folate and antifolate recognition. *Proc Natl Acad Sci.* 2013;110:15180–15188.
24. Shen J, Putt KS, Visscher DW, et al. Assessment of folate receptor-beta expression in human neoplastic tissues. *Oncotarget.* 2015;6:14700–14709.
25. Ross JF, Wang H, Behm FG, et al. Folate receptor type beta is a neutrophilic lineage

marker and is differentially expressed in myeloid leukemia. *Cancer.* 1999;85:348–357.
26. Hu Y, Wang B, Shen J, et al. Depletion of activated macrophages with a folate receptor-beta-specific antibody improves symptoms in mouse models of rheumatoid arthritis. *Arthritis Res Therapy.* 2019;21:143.
27. Nakashima-Matsushita N, Homma T, Yu S, et al. Selective expression of folate receptor beta and its possible role in methotrexate transport in synovial macrophages from patients with rheumatoid arthritis. *Arthritis Rheum.* 1999;42:1609–1616.
28. Wu D, Zhang P, Ma J, et al. Serum biomarker panels for the diagnosis of gastric cancer. *Cancer Med.* 2019;8:1576–1583.
29. Zhou Y, Unno K, Hyjek E, et al. Expression of functional folate receptors in multiple myeloma. *Leukemia lymphoma.* 2018;59:2982–2989.
30. Kurkjian C, LoRusso P, Sankhala KK, et al. A phase I, first-in-human studyto evaluate the safety, pharmacokinetics (PK), and pharmacodynamics (PD) ofIMGN853 in patients (Pts) with epithelial ovarian cancer (EOC) and other FOLR1-positive solid tumors. *J Clin Oncol.* 2013;31(15 Suppl.):2573.
31. Reddy JA, Dorton R, Bloomfield A, et al. Pre-clinical evaluation of EC1456, a folate-tubulysin anti-cancer therapeutic. *Sci Rep.* 2018;8:8943.
32. Banerji U, Garces AHI, Michalarea V, et al. An investigator-initiated phase I study of ONX-0801, a first-in-class alpha folate receptor targeted, small molecule thymidylate synthase inhibitor in solid tumors. *J Clin Oncol.* 2017;35(15 suppl):2503.
33. Desmoulin SK, Wang Y, Wu J, et al. Targeting the proton-coupled folate transporter for selective delivery of 6-substituted pyrrolo[2,3-d]pyrimidine antifolate inhibitors of de novo purine biosynthesis in the chemotherapy of solid tumors. *Mol Pharmacol.* 2010;78:577–587.
34. Golani LK, George C, Zhao S, et al. Structure-activity profiles of novel 6-substituted pyrrolo[2,3-d]pyrimidine Thienoyl antifolates with modified amino acids for cellular uptake by folate receptors alpha and beta and the proton-coupled folate transporter. *J Med Chem.* 2014;57:8152–8166.
35. Golani LK, Wallace-Povirk A, Deis SM, et al. Tumor targeting with novel 6-substituted pyrrolo [2,3-d] pyrimidine antifolates with heteroatom bridge substitutions via cellular uptake by folate receptor alpha and the proton-coupled folate transporter and inhibition of de novo purine nucleotide biosynthesis. *J Med Chem.* 2016;59:7856–7876.
36. Kugel Desmoulin S, Wang L, Hales E, et al. Therapeutic targeting of a novel 6-substituted pyrrolo [2,3-d]pyrimidine thienoyl antifolate to human solid tumors based on selective uptake by the proton-coupled folate transporter. *Mol Pharmacol.* 2011;80:1096–1107.
37. Ravindra M, Wilson MR, Tong N, et al. Fluorine -substituted pyrrolo[2,3-d]pyrimidine analogues with tumor targeting via cellular uptake by folate receptor alpha and the proton-coupled folate transporter and inhibition of de novo purine nucleotide biosynthesis. *J Med Chem.* 2018;61:4228–4248.
38. Wang L, Cherian C, Desmoulin SK, et al. Synthesis and biological activity of 6-substituted pyrrolo[2,3-d]pyrimidine thienoyl regioisomers as inhibitors of de novo purine biosynthesis with selectivity for cellular uptake by high affinity folate receptors and the proton-coupled folate transporter over the reduced folate carrier. *J Med Chem.* 2012;55:1758–1770.
39. Wang L, Cherian C, Desmoulin SK, et al. Synthesis and antitumor activity of a novel series of 6-substituted pyrrolo[2,3-d]pyrimidine thienoyl antifolate inhibitors of purine biosynthesis with selectivity for high affinity folate receptors and the proton-coupled folate transporter over the reduced folate carrier for cellular entry. *J Med Chem.* 2010;53:1306–1318.
40. Wang L, Wallace A, Raghavan S, et al. 6-Substituted pyrrolo[2,3-d]pyrimidine thienoyl regioisomers as targeted antifolates for folate receptor alpha and the proton-coupled folate transporter in human tumors. *J Med Chem.* 2015;58:6938–6959.
41. Wang Y, Cherian C, Orr S, et al. Tumor-targeting with novel non-benzoyl 6-substituted straight chain pyrrolo[2,3-d]pyrimidine antifolates via cellular uptake by folate receptor alpha and inhibition of de novo purine nucleotide biosynthesis. *J Med Chem.* 2013;56:8684–8695.
42. Deng YJ, Wang YQ, Cherian C, et al. Synthesis and discovery of high affinity folate receptor-specific glycinamide ribonucleotide formyltransferase inhibitors with antitumor activity. *J Med Chem.* 2008;51:5052–5063.
43. Meanwell NA. Synopsis of some recent tactical application of bioisosteres in drug design. *J Med Chem.* 2011;54:2529–2591.
44. Maestro, Schrödinger Release 2016-4; Schrödinger, LLC: New York, NY; 2016.
45. Chen C, Ke JY, Zhou XE, et al. Structural basis for molecular recognition of folic acid by folate receptors. *Nature.* 2013;500(7463):486–489.
46. Smart BP, Pan YH, Weeks AK, Bollinger JG, Bahnson BJ, Gelb MH. Inhibition of the complete set of mammalian secreted phospholipases A(2) by indole analogues: a structure-guided study. *Bioorgan Med Chem.* 2004;12:1737–1749.
47. Flintoff WF, Davidson SV, Siminovitch L. Isolation and partial characterization of three methotrexate-resistant phenotypes from Chinese hamster ovary cells. *Somatic Cell Genet.* 1976;2:245–261.
48. Wong SC, Proefke SA, Bhushan A, Matherly LH. Isolation of human cdnas that restore methotrexate sensitivity and reduced folate carrier activity in methotrexate transport-defective chinese-hamster ovary cells. *J Biol Chem.* 1995;270:17468–17475.
49. Deng YJ, Zhou XL, Desmoulin SK, et al. Synthesis and biological activity of a novel series of 6-substituted thieno[2,3-d]pyrimidine antifolate inhibitors of purine biosynthesis with selectivity for high affinity folate receptors over the reduced folate carrier and proton-coupled folate transporter for cellular entry. *J Med Chem.* 2009;52:2940–2951.
50. Dekhne AS, Shah K, Ducker GS, et al. Novel pyrrolo[3,2-d]pyrimidine compounds target mitochondrial and cytosolic one-carbon metabolism with broad-spectrum antitumor efficacy. *Mol Cancer Ther.* 2019;18:1787–1799.
51. Flintoff WF, Nagainis CR. Transport of methotrexate in Chinese hamster ovary cells: a mutant defective in methotrexate uptake and cell binding. *Arch Biochem Biophys.* 1983;223(2):433–440.